Femtosecond Laser-Written Integrated Components for Future All-Fibre Mid-Infrared Laser Systems

By

Gayathri Bharathan

A thesis submitted to Macquarie University

for the degree of Master of Research

Department of Physics and Astronomy

February 2018

MACQUARIE
University
SYDNEY·AUSTRALIA

Examiner's Copy

Typeset in LaTeX 2_ε.

Except where acknowledged in the customary manner, the material presented in this thesis is, to the best of my knowledge, original and has not been submitted in whole or part for a degree in any university.

Gayathri Bharathan

Acknowledgements

I am penning this note of thanks to extend my sincere gratitude towards the remarkable individuals who have supported and helped me throughout my period of study at Macquarie University. It has been a time of intense learning for me, not only in the scientific field but also on a personal level.

First and foremost, I wish to thank my principal supervisor Dr. Alex Fuerbach for giving me the opportunity to pursue research at Macquarie University, Australia. His valuable guidance and continuous encouragement have been a constant inspiration for my studies. In addition, I would like to thank my co-supervisors, Dr. Stuart Jackson and Dr. Darren Hudson, for their guidance and extended support in the course of my research. All my supervisors motivation and immense knowledge always helped me during the research and writing this thesis.

Besides supervisors, I would like to acknowledge the valuable inputs from my colleague and friend Dr. Robert Woodward, who contributed to many fruitful discussions which always helped to shape my research work.

I am grateful to encouraging and always enthusiastic friend Dr. Matthew Collins, who was always keen to know what I was doing and how I was proceeding. I also appreciate his support he had extended me along the way.

With a special mention to Dr. Martin Ams and Sergei Antipov, who transferred me their knowledge on direct femtosecond inscription. It was fantastic to have the opportunity to work a majority of my research using the facilities at the OptoFab node of the Australian National Fabrication Facility.

I would especially like to thank Dr. Joanne Dawson, the Master of Research coordinator, for the timely helps she had extended during this program.

My sincere thanks also goes to my colleagues and friends: Dr. Michael Withford, Dr. Peter Dekker, Dr. Simon Gross, Dr. Alex Arriola, Dr. Benjamin Johnston, Alex Stokes, Anita Verinder, Tom Fewchuk, Thomas Gretzinger, Glen Douglass, Christoph Wieschendorf, Saheed Oladipupo Fashola, Andrew Ross-Adams, Blacke Entwisle, Michelle Witford, Soumya Sarang and Sarath Raman Nair. It was a great pleasure to work with you.

I am grateful to the God almighty for his unconditional blessings. And finally, last but not the least, I would like to express my sincere gratitude towards my inspiring parents, lovely sister and a fantastically supportive partner who have provided me with moral and emotional support in my life.

Thanks for all your encouragement!
Gayathri

List of Publications

- G. Bharathan, R.I. Woodward, M. Ams, D.D. Hudson, S.D. Jackson, A. Fuerbach: "Direct inscription of Bragg gratings into coated fluoride fibers for widely tunable and robust mid-infrared lasers", Optics Express 25, 30013 (2017).

- G. Bharathan, R. I. Woodward, M. Ams, D. D. Hudson, S. D. Jackson, A. Fuerbach: "Widely Tunable Mid-Infrared All-Fibre Lasers Based on Mechanically Robust Fibre Bragg Gratings", The 3rd Australian New Zealand Conference on Optics (ANZCOP), Queenstown, New Zealand (2017).

- A. Fuerbach, G. Bharathan, S. Antipov: "Line-by-line femtosecond FBG inscription for innovative fiber lasers", Invited talk, Bragg Gratings, Photosensitivity and Poling in Glass Waveguide (BGPP), OSA Advanced Photonics Congress, Zurich, Switzerland (2018).

Abstract

Lasers emitting at mid-infrared (mid-IR) wavelengths in the 2.5–5 μm range are essential for various applications as this spectral region coincides with the vibrational-rotational absorption lines of many important atmospheric gases and liquid water. Fibre lasers are an efficient way to generate light at mid-IR wavelengths. However, mid-IR fibre laser technology is still in its infancy, mainly due to the non-existence of fibre coupled optical components to create all-fibre cavities, which severely limits their practical applications.

This thesis investigates the feasibility of using a femtosecond laser to fabricate integrated components such as fibre Bragg gratings (FBGs), couplers and splitters which can add a new perspective for mid-IR all-fibre lasers. We report the development of a widely tunable (37 nm) all-fibre mid-IR laser based on a mechanically robust FBG which was inscribed through the polymer coating of a double clad fluoride fibre by focusing femtosecond laser pulses into the core of the fibre without the use of a phase mask. In a further step, the possibility of using on-chip optical couplers inscribed in fluoride and chalcogenide glasses is also investigated to pave the way for the realization of compact and robust mid-IR fibre laser systems for real-world applications in spectroscopy and medicine.

Contents

List of Figures

List of Tables

1

Introduction

Laser technology has had a tremendous impact in today's world. From underwater optical communication links that span across continents and provide high data rates to advancements in modern opto-electronics industry, from measurements to analysis, from manufacturing to medicine, from research to entertainment. In fact, when the laser was first invented, scientists described it as a "solution looking for a problem". In the past 67 years, the laser has turned out to be one of the most useful devices ever invented and has led to several revolutionary changes in various fields. Research still continues in the field of lasers and we can only wonder what the coming years will bring to the world.

1.1 Main objective

The topic of research presented in this thesis is concerned with the mid-infrared (mid-IR) region of the electromagnetic spectrum especially with the range 2.5–4 μm. The photon energies (~0.3–0.5 eV) of these wavelengths overlap with the fundamental vibrational modes

of many molecules, leaving distinctive spectral fingerprints that can enable the sensitive detection of specific molecules [12, 13]. For example, mid-IR lasers in the region 3–3.5 μm overlap with the methane absorption lines whereas the spectral region 2.5–2.8 μm overlaps with the CO_2 absorption lines [14]. This mid-IR fingerprint absorption spectrum is unique for a specific compound. That means, it can be used for the identification of specific molecules within a sample by comparing the measured mid-IR absorption spectrum with know molecular mid-IR spectra. Similarly, water has a strong absorption due to the asymmetric and symmetric O-H stretching vibrations at wavelengths at 2.662 μm and 2.734 μm respectively [15]. A major application of targeting this water absorption lies in laser microsurgery for minimally invasive ablation of human tissue. Hence, the above mentioned mid-IR light is relevant for applications such as hazardous chemical detection, atmospheric monitoring, or medicine. The search for a compact and high beam quality laser for these applications at these wavelengths led to the development of fibre lasers based on fluoride glasses. However, the non-existence of fibre coupled optical elements to form an all-fibre laser cavity limits their applicability. The work presented in this thesis takes further steps towards the development of future all-fibre mid-IR laser systems by fabricating new optical components such as fibre Bragg gratings and directional couplers in mid-IR compatible glasses.

1.2 Layout of the thesis

This thesis is divided into six chapters. The current chapter is intended to provide a brief introduction to the thesis topic and to provide a motivation for the work.

Chapter 2 details basic background information on optical fibres and their application in forming a fibre laser cavity. It also lays out the development and applications of mid-IR fibre lasers.

Chapter 3 provides an overview of the femtosecond laser direct-write technique. This method utilises an ultrafast pulsed laser that is focused into various glass materials to inscribe micro-structures in three dimensions which are then used in our experiments.

Chapter 4 begins with a basic overview of fibre Bragg gratings (FBGs) and elaborates on procedures, methods and equipment for the fabrication of FBGs. It then describes uniform FBGs fabricated within various fibres. Later, it discusses the development of a tunable all-fibre mid-IR laser system using mechanically robust FBGs as well as the integration of

chirped fibre Bragg gratings into a mid-IR fibre laser cavity.

Chapter 5 is dedicated to femtosecond laser inscribed integrated optical components like directional couplers in fluoride and chalcogenide glasses. This chapter investigates the feasibility of using these directional couplers in future all-fibre mid-IR laser systems.

The thesis concludes with a summary in Chapter 6 and an outlook towards future research directions which will build on the work presented in this thesis.

2

Background on Mid-Infrared Fibre Laser Technology

This chapter discusses the topic of fibre lasers for the mid-infrared (mid-IR) region. As mentioned in the previous chapter, this spectral region is of particular interest for many important applications. This chapter begins with a brief section on optical fibres and their use to form a laser cavity. A summary of previous work in mid-IR fibre lasers follows and the chapter concludes with a discussion on true all-fibre systems.

2.1 Optical fibres

An optical fibre is a transparent and flexible waveguide that is composed of a material with a higher refractive index (n_1) in its center, called the core. This core is surrounded by a region of lower index of refraction (n_2) named cladding. This permits light to propagate through the fibre via total internal reflection, which is a physical phenomena that can be described based

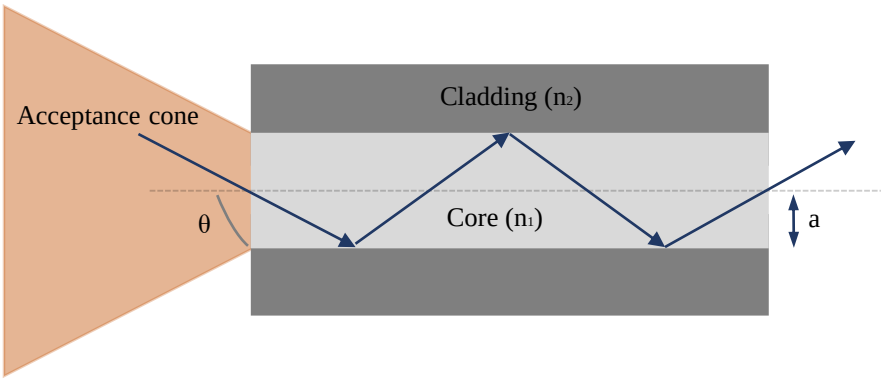

Figure 2.1: Cross section of a step index optical fibre.

on ray optics theory. Figure 2.1 illustrates the geometry of a step index optical fibre, where a is the core radius. The difference between core and cladding refractive indices leads to a set of ray angles determining the acceptance cone (2θ) which guide light through the core via total internal reflection. The sine of the half angle of this acceptance cone represents the numerical aperture (NA) of the fibre as given by [16]

$$NA = \sin(\theta) = \sqrt{n_1^2 - n_2^2}. \tag{2.1}$$

Solving Maxwell's equations for a cylindrical geometry reveals various solution of light propagation within the fiber called 'Modes'. Individual modes have a unique spatial distribution of the electric field, and the lowest order modes that are commonly present in fibres are shown in Figure 2.2. For most laser applications, the lowest order LP_{01} mode (fundamental mode), that closely resembles a Gaussian profile is preferred. The V number of a fibre is defined as,

$$V = \frac{2\pi}{\lambda} aNA. \tag{2.2}$$

For V values < 2.405, the fibre only supports the fundamental mode [16]. Therefore, at a given wavelength of light, the radius and numerical aperture of the fibre are typically chosen such that $V < 2.405$, to yield single mode operation.

2.1.1 Silica vs fluoride fibres

Optical fibres are predominantly fabricated from glasses. Due to its favourable properties like high damage threshold, chemical stability, high purity and the possibility to introduce doping materials at high concentrations into the glass matrix, fused silica is the dominant material in fibre optics. Silica fibres are highly transparent for wide wavelength ranges in

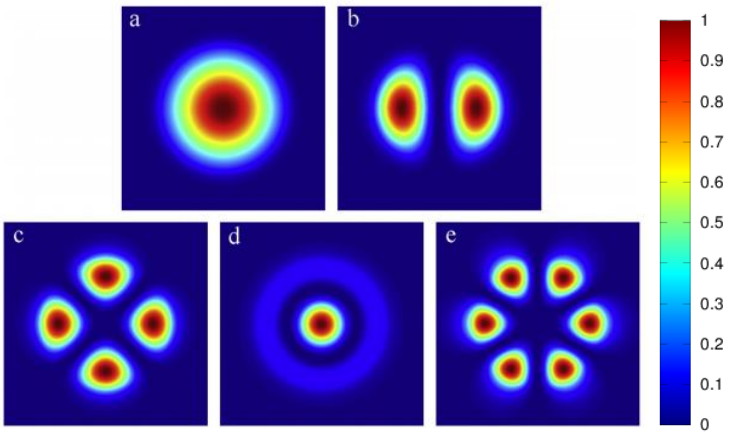

Figure 2.2: Mode field distributions of intrinsic modes in Fiber (a) LP-01, (b) LP-11, (c) LP-21, (d) LP-02 and (e) LP-31 [1]

the visible and near-IR region, especially around 1.55 μm. Since light at 1.55 μm propagates through silica fibres with very low attenuation (0.2 dB/km), it can be used as a medium for long distance telecommunication. However, above ~2 μm wavelengths the performance of silica fibres deteriorates and losses increase dramatically. The photon energy is transferred from electromagnetic energy to vibrational energy through the "multi-phonon absorption" process which leads to strong attenuation at wavelengths greater than 2 μm in both passive as well as active silica fibres.

Moving to longer wavelengths near 3 μm, silica glass becomes virtually opaque and thus unsuitable for the development of fibre laser sources. The high phonon energy of silica prohibits mid-IR laser transitions since phonons cause strong non-radiative relaxation of excitation, rather than radiative emission. Addressing this problem is an acute challenge for fundamental materials science. In order to achieve low phonon energies, the host lattice needs to have heavy atoms bound together with bonds that display low spring constants (i.e. weakly bound) [2]. Findings reveal that fluoride and chalcogenide glasses have low phonon energy, good mid-IR transparency and are chemically stable. ZBLAN (ZrF_4-BaF_2-LaF_3-AlF_3-NaF) is considered to be the most stable heavy metal fluoride glass and represents an excellent host for rare-earth ions. This glass has been extensively used for its benefits such as wide transparency window and low phonon energy (565 cm^{-1}) when compared to silica fibre (1100 cm^{-1}) [2, 17]. Figure 2.3 reveals the propagation loss spectrum of un-doped silica vs un-doped ZBLAN fibre in the near and mid-IR. The low phonon energy of ZBLAN allows for light propagation up to 4 μm [2].

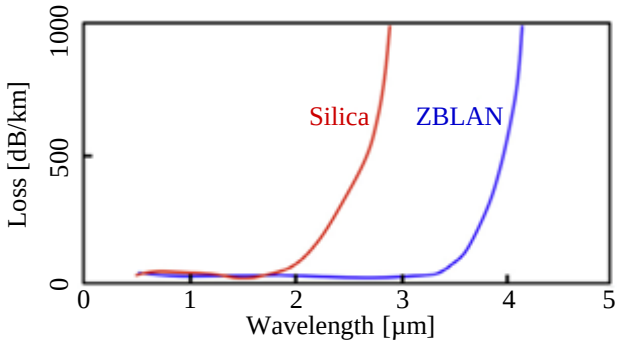

Figure 2.3: Propagation loss spectrum of undoped silica vs undoped ZBLAN fibre [2].

2.2 Fibre lasers

One of the most revolutionary inventions in science is the LASER (Light Amplification by Stimulated Emission of Radiation). A pump source, a gain medium, and an optical feedback element are the fundamental components to form a laser cavity.

Even though there are countless cavity designs to realise a laser system, fibre lasers are efficient and versatile waveguide devices that utilize an actively doped optical fibre as their gain medium, as depicted in Figure 2.4. Generally, those fibres are doped with rare-earth elements like Erbium (Er^{3+}), Ytterbium (Yb^{3+}), Thulium (Tm^{3+}), or Holmium (Ho^{3+}) based on the wavelength of the specific application. In the simplest case, the ~4% Fresnel reflection from the perpendicularly cleaved input and output facets of the fibre act as a low reflectivity broadband mirrors that form a linear cavity. Electrons are excited to a higher energy state by an optical pump field that is coupled into the doped fibre. Laser light is then emitted through stimulated emission and due to the optical feedback, a coherent laser beam is emitted at both ends of the fibre as shown in Figure 2.4. However, the performance of the laser depends on

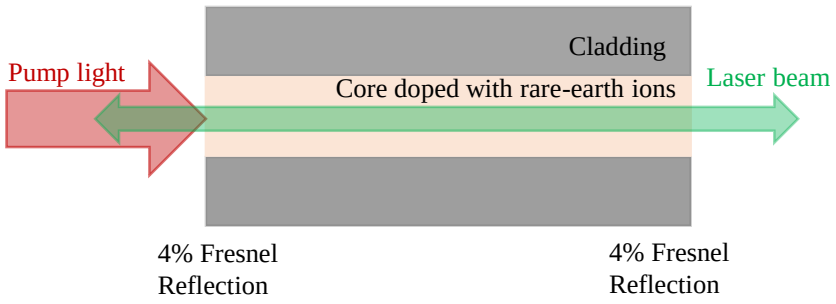

Figure 2.4: Schematic of a fibre laser. In this example, the doped core acts as the gain medium and Fresnel reflections provide optical feedback.

the precise parameters of the laser. This simplest form of the fibre laser can be improved by incorporating coatings or mirrors to one or both sides of the fibre or by using fibre Bragg gratings (FBGs), which are in-fibre reflectors that can help to achieve higher efficiencies as will be demonstrated in Chapter 4.

2.2.1 Double clad optical fibres

Before moving on to mid-IR fibre lasers, a brief look into a special class of fibres named double clad fibres is required as these are important building blocks of high power laser systems.

The large surface area to volume ratio makes fibre lasers an excellent device to dissipate excess heat produced from high power pumping [18, 19]. However, a few problems can occur when pumping directly into the core of the fibre. Compact high power multi-mode pump diodes typically exhibit fairly poor beam quality and it is challenging to couple their output efficiently into a small fibre core even though the fibre has a favourable geometry. Also, in single-clad fibres the thermal effects can lead to complexities in the alignment of optical devices at higher pump powers [3]. This requires the use of pump sources with diffraction-limited beam quality. An evident method to overcome these issues is to use the double-clad fibre geometry.

As the name suggests, a double clad fibre has two claddings surrounding the core to form a fibre. The core of the fibre is doped with the rare earth elements and is designed specifically to operate in the fundamental transverse mode. This core is surrounded by a cladding with a larger diameter, to guide the pump light. The much easier coupling of the pump light to the first cladding compared to the core is the major benefit of this structure since the first cladding is much larger than the core area and has a high NA typically (~0.5). When the fibre is pumped, the modes guided in the cladding intersect with the doped core. Consequently, the effective pump absorption is reduced and longer lengths of fibre are typically required. Lastly, the single mode emission from the small core compared to the larger multimode cladding results in an enhancement in the brightness of the laser light thereby creating a diffraction limited output beam [20],[3]. High beam quality and great reliability due to the waveguide effect are key requirements for various applications in medicine, defence, and materials processing.

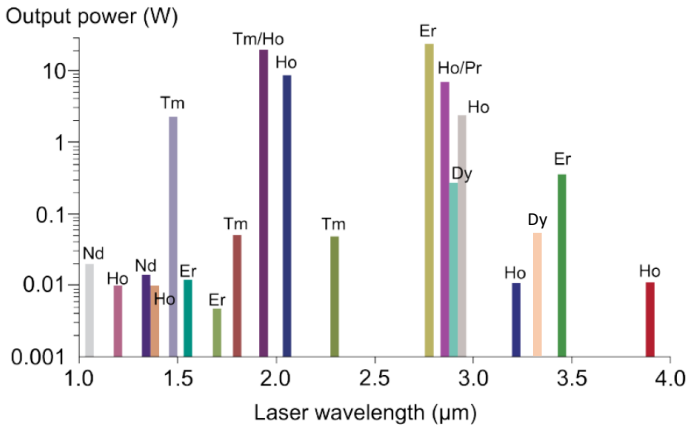

Figure 2.5: Various rare-earth ions that have been successfully doped into ZBLAN fibres to achieve lasing [3].

2.2.2 Active dopants for generating mid-infrared light

Previous sections have provided a basic understanding of fibre lasers. This section discusses various types of rare-earth ions being used to generate light at mid-IR wavelengths.

Many groups have studied various rare-earth doped ZBLAN fluoride fibre lasers at long wavelengths, where silica fibres cannot be used. In 1989, Allen *et al* reported a Tm^{3+} doped ZBLAN fibre laser emitting at 2.3 μm [21]. Later, Brinkley *et al* and Henderson-Sapir *et al* demonstrated emission at 2.7 μm and 3.5 μm from Er^{3+} doped ZBLAN fibres [22, 23]. It was also demonstrated that Ho^{3+} doped ZBLAN fibres can be used for building fibre lasers at 2.9 μm, 3.2 μm and 3.9 μm wavelengths [24–26]. More recently, Majewski *et al* reported a highly efficient Dy^{3+} doped fluoride fiber laser with a maximum emission wavelength of 3.26 μm [27].

High brightness semiconductor pumps and new fibre designs drive the power scaling of fibre lasers in the mid-IR. Doped ZBLAN fibre lasers have highly benefited from these breakthroughs. The highest output powers of infrared ZBLAN fiber lasers at different wavelengths are summarized in Figure 2.5 [3].

In the remainder of this chapter, we will focus on holmium, a rare-earth element which is capable of emitting around 3.0 μm, a wavelength regime that is of particular importance for medicine. When mid-IR fibre lasers operating near 3 μm are considered, the reported maximum slope efficiencies of semiconductor diode pumped Er^{3+} and Ho^{3+} doped fibre lasers are 35.4% and 32% respectively [28–30]. However, mid-IR erbium-doped fluoride fiber lasers emit around 2.8 μm, a wavelength that lies directly in the region of high water

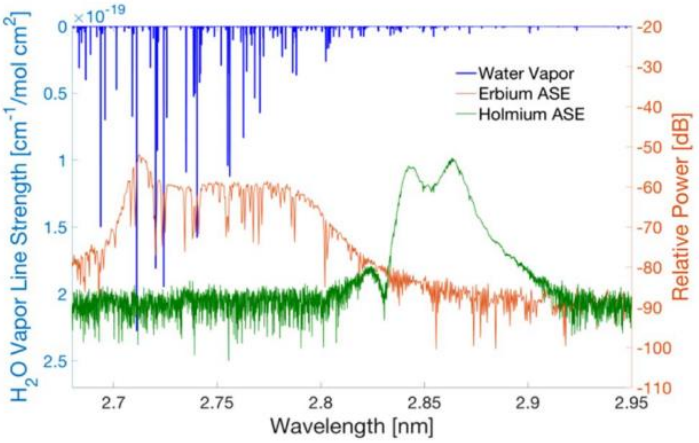

Figure 2.6: Water vapor absorption lines (blue) overlaid with the amplified spontaneous emission (ASE) spectra of erbium-doped ZBLAN (orange) and holmium-doped ZBLAN (green). [4].

vapor absorption. This absorption has previously limited the achievable bandwidth and laser output power and poses a serious problem for free space transmission [4]. In the following section, we will study the energy levels of holmium ions in detail.

Holmium based fibre lasers

Mid-IR fiber lasers that use Ho^{3+} as the gain medium overcome the limitations of erbium based fibre lasers when pumped at 1.15 μm wavelength. Holmium allows the central emission wavelength to shift to nearly 2.9 μm which avoids the strong water vapor lines as shown in Figure 2.6 [4]. Figure 2.7(a) depicts that the main problem with using holmium as a gain medium is the long $^5I_7$ lower laser level lifetime (τ=12.5 ms) which is longer than the $^5I_6$ upper laser lifetime (τ=3.5 ms) [4]. To circumvent this, Ho^{3+} doped fibres can be co-doped with praseodymium (Pr^{3+}) ions, which serves to depopulate the holmium lower laser level and force a straightforward four-level laser system (see Figure 2.7(b)). Through this highly resonant energy transfer process the Pr^{3+} ions reduce the Ho^{3+} lower laser level lifetime to microsecond durations, allowing efficient lasing on this transition [4]. Holmium-praseodymium lasers demonstrate several key advantages related to the laser stability and performance [20].

2.3 Mid-IR all-fibre lasers

Fibre lasers with emission wavelengths at the range of 2.5–5 μm correspond to photon energies that overlap with the strong vibrational molecular resonances of most common constituents

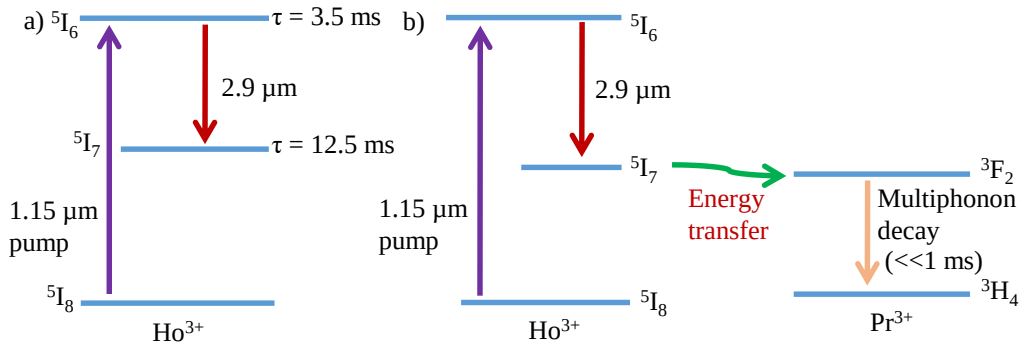

Figure 2.7: (a) Energy level diagram of Ho^{3+} ions and (b) the addition of Pr3+ to Ho3+ allows an energy transfer the process from the $^5I_7$ to the $^3F_2$ level which then quickly decays via multiphonon decay.

of atmospheric gases such as carbon dioxide (CO_2), carbon oxide (CO) and methane (CH_4) [12], as well with those of liquid water contained in biological tissues [15]. As water is the major constituent of human tissue, lasers emitting mid-IR wavelengths are strongly absorbed by water, which causes rapid heating, rapid expansion and ablation resulting in the precise cutting of the tissue [2]. As previously mentioned, apart from tissue interaction applications, 2.9 µm mode-locked (a technique used to generate ultrashort pulses) and/or tunable fibre lasers also have the potential to become turnkey systems for ultrasensitive, broadband molecular spectroscopy.

Several advantages including high beam quality, flexible beam delivery, and compact size, make fibre lasers the ideal light source for most applications. Fibre lasers have thus become one of the most common types of lasers, in the near-IR region [31]. In contrast, mid-IR fibre laser technology is still in its infancy, due to the non-existence of fibre coupled optical components to realize all-fibre cavities, which severely limits their applicability.

Most continuous wave (CW) and pulsed fibre lasers that have been demonstrated in the mid-IR regime to date [4, 23, 32] utilize bulk optical elements. However, the incorporation of bulk optical components to the laser cavity adds complexity as well as losses and makes the system less stable and more expensive. A striking feature of an all-fibre laser system is that performance inhibiting intra-cavity absorption by atmospheric gases can be avoided, and the all-fibre geometry removes the requirement of manual alignment of free space optics. The system becomes largely insensitive to vibrations and temperature variations. Furthermore, an all-fibre laser cavity can also help to reduce the cavity losses. Overall, the main benefit of an all-fibre laser system is that it allows turnkey operation to the user with greatly improved

reliability and stability.

The low loss all-fibre Fabry-Perot laser cavity that is formed by directly inscribing FBGs into active fluoride fibres paved the way to an all-fibre laser system at mid-IR region [19, 33, 34]. In the future, chirped fibre Bragg gratings (CFBGs) can become vital components for developing all-fibre ultrafast laser systems in the mid-IR regime as will be discussed in Chapter 4. Additionally, the development of integrated optical components like couplers and wavelength division multiplexers could be a potential route to replace the bulk optical components that are required in a ring laser cavity which is the preferred geometry for ultrafast lasers. Direct femtosecond laser inscription of fibre Bragg gratings and other integrated components for use in future all-fibre mid-IR laser systems, operating at 3 μm is discussed in the coming chapters.

3

Background on the Femtosecond Laser Inscription Process

The capability of femtosecond lasers to directly inscribe features into different transparent glasses opens a new avenue for the development of future mid-IR all-fibre laser systems. This chapter begins with an introduction to femtosecond laser-material interaction, proceeds further on to various modification schemes and concludes with an overview of current research activities in this area and a detailed explanation of the project objectives.

3.1 Femtosecond laser-material interaction

Laser – material interaction can happen in several ways depending on the absorption characteristics of the material, intensity, pulse duration and wavelength or frequency of the laser. In dielectric materials like glasses, the electrons occupy the valence band, while the conduction band is empty. An energy gap, E_g separates the valence band from the conduction band. If

the electrons in the valence band gain enough energy from an external radiation field, they can transfer from the valence band to the conduction band to become quasi-free electrons. This process requires an external energy that exceeds the bandgap energy (E_g). For most glasses, a single photon of visible light does not possess enough energy to elevate an electron from the valence band to the conduction band. In this case, nonlinear absorption processes are required to promote valence band electrons to the conduction band. There are two classes of nonlinear excitation mechanisms that play a role in this process, photoionisation and avalanche ionisation [5].

3.1.1 Photoionisation

The direct excitation of electrons from the valence band to the conduction band of a material under the influence of an optical field is known as photoionisation. In glasses, several photons are typically required simultaneously to promote an electron from the valence band to the conduction band since a single photon of visible light does not have enough energy to excite an electron. Depending on the laser's frequency and intensity, there are two different regimes of photoionisation, the tunnelling ionization regime and the multi-photon ionisation regime [5].

In the tunnelling ionization regime, the Coulomb well which binds a valence electron to its parent atom is suppressed by the electric field of the laser. If the electric field is very strong, the Coulomb well can be suppressed enough so that the bound electron can tunnel through the barrier and become free, as illustrated schematically in Figure 3.1(a). This type of nonlinear ionization dominates for strong laser fields and low laser frequencies [5].

At high laser frequencies (but still below that required for single photon absorption) nonlinear ionization occurs due to the simultaneous absorption of multiple photons by an electron, as shown in Figure 3.1(b) [5]. In this case, the total absorbed energy of all the m photons that interact with the single electron must have an energy that exceeds the bandgap energy, i.e, $mh\nu \geq E_g$ with E_g being the material's bandgap, ν the frequency of light and h Planck's constant.

3.1.2 Avalanche ionisation

Besides tunneling ionisation and multi-photon ionisation, an electron already present in the conduction band can absorb multiple photons sequentially, moving to higher energy states in

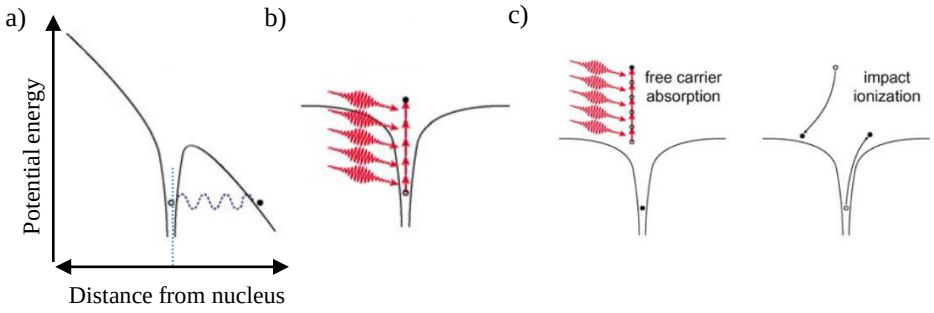

Figure 3.1: Nonlinear photoionisation processes during femtosecond laser inscription (a) tunneling ionisation, (b) multi-photon ionisation and (c) avalanche ionisation [5]. The vertical axis shows the potential energy of an electron and horizontal axis shows the distance from nucleus.

the conduction band as shown in Figure 3.1(c). A bound electron from the valence band can then be promoted to the conduction band via impact ionisation. These two excited electrons can now again promote new electrons into the conduction band by absorbing energy, forming an avalanche ionisation process [5]. The seed electrons to initiate the avalanche process are mainly provided either by thermally excited carriers, by easily ionized impurity or defect states, or by carriers that are directly photo-excited by multi-photon or tunneling ionization [5]. The avalanche ionisation process subsequently leads to the growth in free electron density that forms a plasma. This high-density plasma strongly absorbs laser energy by free carrier absorption. Avalanche ionisation is the dominating process when the laser pulse durations are a few hundred fs and longer. Femtosecond laser pulses can photoionise electrons during the leading edge of the pulse providing seed electrons for avalanche ionisation to occur during the rest of the pulse [5, 35].

3.2 Modification schemes

In this section, we discuss the material modifications can occur as a result of the non-linear photoionisation processes. After a high-density electron plasma has been formed, the energy of the electrons is transferred to the lattice,. This typically results in a permanent modification of the refractive index, thus enabling the inscription of photonic structures inside various non-photosensitive optical materials. Depending on the incident pulse energy, the femtosecond direct-write technique can induce three types of material modifications: a smooth refractive

index change also known as Type-I modification, a birefringent refractive index change, and a damage modification (void) otherwise called Type-II modification. It should be noted that the change in refractive index produced in the laser-irradiated volume can be positive or negative and depends on the laser and material parameters.

3.2.1 Smooth refractive index / Type-I modification

As mentioned before, when the femtosecond laser energy is absorbed by a material, it will be transferred to the lattice via electron–phonon coupling. This may further lead to rapid heating and structural modification in a small volume of the material at the laser focal point [36]. The generation of a smooth refractive index change or Type-I modification [37] (<90 nJ in silica) is crucial for the development of low loss waveguides. However, the strength of the refractive index change critically depends, amongst other parameters, on the repetition rate of the femtosecond laser. The structural modifications induced by kHz and MHz lasers in BK7 borosilicate glass were investigated by Little *et al* who found that the main cause for the refractive index increase upon MHz irradiation was densification where densification is the collapse of matter into a more close-packed structure and is a displacive transformation, whereas kHz irradiation mainly results in the formation of colour centres [38].

3.2.2 Birefringent refractive index modification

In an intermediate pulse energy regime, it was demonstrated that the modified areas in fused silica contain nanoporous structures that are sensitive to the polarization state of the inscription beam [23, 26, 39]. These nanostructures were found to be self-ordered and periodic (with a size and period as small as 20 nm and 140 nm, respectively) while being oriented in a direction perpendicular to the electric field vector of a linearly polarised femtosecond laser writing beam. This periodically varying material composition found in the irradiated volume gives rise to birefringent refractive index changes [40].

3.2.3 Void / Type-II modifications

At exceedingly high pulse energy levels (~95 nJ in silica), the material experiences damage or void formation which is known as Type-II modification [37]. A localized plasma is formed in the focal volume of the femtosecond laser due to photoionisation process [41]. As plasma density in the focal region increases, the plasma causes a large charge separation resulting in high pressures. This charge separation further leads to a micro explosion within the material

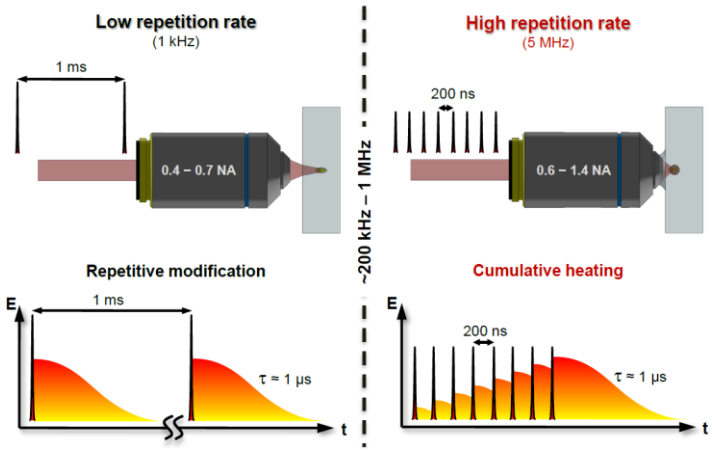

Figure 3.2: The two different femtosecond laser direct-writing regimes. At low repetition rates, every single pulse creates a permanent material change while at high repetition rates cumulative heating occurs [6].

thereby generating a shock wave. Later, this shock wave carries matter and energy away from the focal volume, compressing the surrounding material and leaving a rarified (less dense or hollow core) central region termed a void [41–43].

3.3 Aspects of femtosecond laser inscription

This section discusses the two major aspects of the femtosecond laser direct inscription process. The first concern is the repetition rate of the laser which can greatly influence the material modification. Secondly, the focusing conditions are crucial since nonlinear breakdown occurs in the focal volume of the laser.

3.3.1 Laser repetition rate

Femtosecond laser direct inscription can be divided into two regimes: the low repetition rate regime and the high repetition rate regime. The pulse repetition rates are normally <100 kHz in the low repetition rate regime, for example if a Ti:Sapphire laser operating at 1 kHz is used. In this case, when the first pulse is absorbed in the glass substrate, it locally heats the material and subsequently modifies the glass in the focal volume. The heat produced in the irradiated region will dissipate away (the typical heat diffusion time in glasses is about 1 µs) thereby creating a permanent refractive index modification and the glass cools down to the ambient temperature before the next pulse arrives as schematically shown in the bottom left side of Figure 3.2. In the high repetition rate regime >1 MHz, the time period between

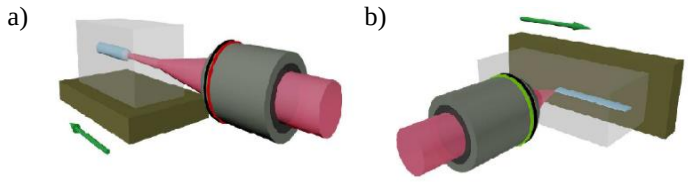

Figure 3.3: Writing geometries for the femtosecond laser direct write method (a) longitudinal (b) transverse. Green arrows indicate the translation direction of the sample. [7]

each single pulse is reduced to the point where heat generated in the focal volume of the laser does not have adequate time to diffuse into the surrounding glass. Hence, heat starts to build up around the focal volume as shown on the right-hand side of Figure 3.2. The heated area starts expanding with an increase in temperature and once the melting point is reached the material becomes permanently modified.

3.3.2 Beam focusing

When inscribing devices with femtosecond lasers using the direct write method, the beam waist of a focused laser pulses is inversely proportional to the NA of the focusing objective and can be expressed as

$$2\omega_0 = \frac{2f\lambda}{\pi w} = \frac{2\lambda}{NA\pi}, \tag{3.1}$$

where ω_0 is the beam waist radius, w is the radius of the beam at the input of the objective, f is the focal length of the objective and NA is its numerical aperture. Care has to be taken when selecting the beam diameter of the inscription laser and the focal length of the focusing objective since the NA depends on both previously mentioned parameters.

Once the focusing conditions have been designed, the desired structures can be inscribed into the sample by scanning the sample through the focal spot of the laser beam. Commonly, there are two writing geometries associated with femtosecond laser inscription of integrated optical elements named as longitudinal (parallel) and transverse (perpendicular) writing geometries. In the longitudinal writing geometry, the sample is translated in the direction of propagation of the laser beam as depicted in Figure 3.3. However, this method is limited by the objective's working distance and the quality of inscription might be affected by spherical aberrations which vary with the depth of focus inside the sample.

In the transverse writing geometry, integrated devices are inscribed in a sample while moving the sample perpendicular to the propagation of the laser beam. This geometry

offers greater flexibility in inscribing structures into a sample with arbitrary length as well as eliminating the limitation of working distance of the objective associated with the longitudinal writing geometry [7].

3.4 Current research activities and project objectives

Researchers have previously fabricated highly reliable and low cost integrated optical devices such as couplers, waveguides and FBGs in various materials like glasses, crystals and polymers using the femtosecond laser direct write technique, for applications in various fields of optics. Williams *et al* have fabricated FBGs with the femtosecond laser direct write technique in fluoride fibres for the development of an all-fibre mid-IR laser system [44, 45]. Arriola *et al* have conducted an experimental study into suitable host materials for inscribing waveguides for mid-IR interferometry [46]. Later, Gross *et al* have developed low loss mid-infrared ZBLAN waveguides and couplers for astronomical applications [11], whereas Gretzinger *et al* reported the fabrication of low-loss single-mode waveguides and couplers in gallium lanthanum sulfide (GLS) using femtosecond lasers [47]. In this thesis we propose that such couplers could also be used for the development of future all-fibre mid-IR ring lasers, see Chapter 5.

The main objective of this work is the fabrication and characterization of integrated optical components and devices such as FBGs and couplers, written into ZBLAN and chalcogenide glasses, using the femtosecond laser direct-write technique to form all-fibre laser cavities. Chapter 4 of this thesis focuses on the fabrication methods to inscribe uniform and chirped fibre Bragg gratings (CFBGs) into silica and in particular fluoride fibres with and without a polymer jacket. It also presents in detail a tunable mid-IR all-fibre laser system that uses a mechanically robust FBG. Chapter 5 outlines the development and characterization of integrated couplers fabricated in ZBLAN and GLS using the femtosecond laser direct-write technique for future mid-IR all-fibre laser systems.

4

Femtosecond Laser Inscription of Fibre Bragg Gratings for Fibre Laser applications

The theoretical background knowledge on femtosecond laser inscription was presented in the previous chapter. This chapter elaborates on the procedures, methods and the equipment employed in the fabrication of fibre Bragg gratings (FBGs) using the femtosecond laser direct write technique. The first part of the chapter gives a brief introduction to fibre Bragg gratings, various fabrication methods and details of the microfabrication setup used in this work. The second section covers the experimental results and contains a discussion of FBGs fabricated in silica and ZBLAN fibres. The final section of this chapter details the practical use of femtosecond laser inscribed uniform and chirped gratings for the realisation of robust tunable all-fibre mid-IR lasers and the development of Fabry-Perot cavities with improved Q-factor.

4.1 Fibre Bragg gratings (FBGs)

Fibre Bragg gratings are spectrally selective reflectors that are formed from periodic refractive index modifications to the fibre core. This technology had a tremendous impact on optical fibre sensing and telecommunications. FBGs are also employed extensively in fibre lasers to achieve narrow linewidth operation. The following sections elaborate the various types of FBGs used in our experiments.

4.1.1 Uniform fibre Bragg gratings

Uniform fibre Bragg gratings (UFBGs/FBGs) are reflective structures inscribed within the core of an optical fibre having a periodic perturbation of the effective refractive index over a certain length (typically 10–15 mm). This refractive index variation leads to the reflection of light in a narrow band of wavelengths, for which the Bragg condition is satisfied. This means that if light is injected from a broadband source to the optical fibre with an FBG inscribed, only light within a very narrow spectral region centered at the Bragg wavelength (λ_B) will be reflected back by the grating as illustrated in Figure 4.1. At λ_B, the light reflected from the interface between the different dielectric slabs of dissimilar refractive index of the grating are in phase and thus add up constructively. The remaining light will continue propagating inside the optical fibre without experiencing any loss in an ideal FBG [48]. The Bragg wavelength is defined by the physical pitch (period) of the microstructure (Λ) and the effective index of refraction (n_{eff}) of the core mode

$$\lambda_B = 2\Lambda n_{\text{eff}}. \tag{4.1}$$

4.1.2 Chirped fibre Bragg gratings

In chirped fibre Bragg gratings (CFBGs), the period is made to vary along the length of the fibre. Such gratings can reflect a broader range of wavelengths and introduce wavelength dependent group delay and dispersion as depicted in Figure 4.1. CFBGs can be used for broadband sensing and dispersion management in lasers or as broader bandwidth reflectors compared to uniform FBGs for continuous wave (CW) lasers.

In the final section of this chapter, the development of a tunable mid-IR all-fibre CW laser systems using uniform FBGs and the improvement in its slope efficiency using a CFBG will be demonstrated.

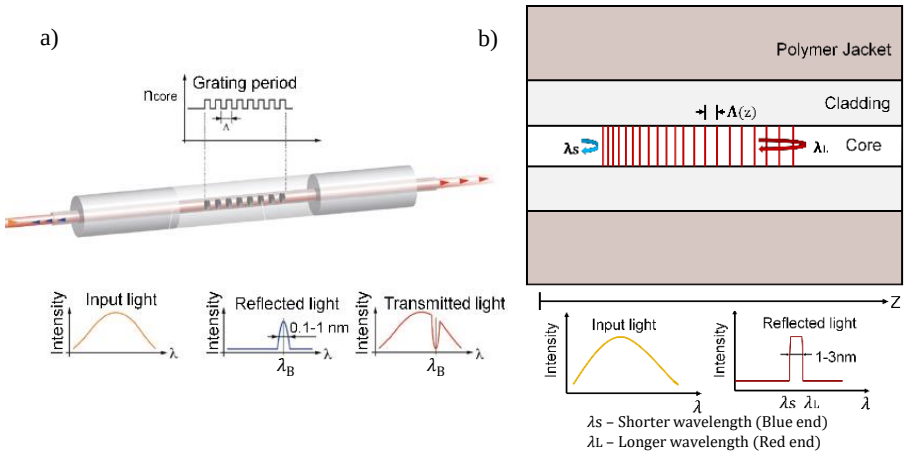

Figure 4.1: (a) Uniform [8] and (b) chirped fibre Bragg gratings and their spectral response.

4.2 Direct inscription of fibre Bragg gratings

The conventional method used for FBG inscription is the use of photosensitive fibres [48]. Typically, a germanium or boron doped silica fibre exhibits a permanent increase in refractive index upon single photon or two-photon absorption of ultraviolet light [49]. The periodicity of the inscribed refractive index perturbation is provided by exposing the core to the interference pattern formed by two ultra-violet (UV) laser beams or from the +1 and -1 diffraction orders from a phase-mask [50]. The dependence on a specific expensive phase mask to define the period remains a limitation of the phase mask technique.

As illustrated in the previous chapter, the multi-photon absorption and ionisation processes caused by femtosecond laser pulses can lead to a permanent refractive index modification in materials. This concept has been effectively utilised to fabricate optical devices in several materials. In 1996, Davis *et al* showed that a pathway of refractive index modification could be inscribed in various glass samples by translating the sample with respect to a femtosecond laser beam [50]. The first FBG inscribed with femtosecond laser pulses was later demonstrated by Mihailov *et al* by irradiating a standard Ge-doped silica fibre through a phase mask, which resulted in a strong Bragg resonance (-45 dB transmission dip) caused by an index modulation of $\Delta n = 1.9\times10^{-3}$ [51]. More recently, it was shown that the femtosecond laser phase mask technique could also be used to inscribe FBGs into active ZBLAN fibres to realize all-fibre single wavelength mid-IR laser systems around 3 μm [19, 52]. However, in all these reports, the reliance on a specially designed phase mask still limits the flexibility and costs of this inscription method. Besides that, these methods require chemical or mechanical stripping of the polymer coating of the fibre before the inscription process, which reduces the

mechanical strength of the fibre and/or requires complex recoating methods.

4.2.1 Point-by-point inscription method

In addition to the more conventional techniques for producing a modulated refractive index perturbation within the core of the optical fibre, which include the use of phase masks as well as interferometric techniques, femtosecond laser inscription of FBGs has also successfully been demonstrated using a highly flexible point-by-point (PbP) approach, initially in a standard telecommunication fibre [53]. The major advantage of this technique is that it does not require a phase mask, yet an arbitrary longitudinal refractive index modulation profile can be inscribed into the core of an optical fibre simply by programming the desired pattern into the movement of an air-bearing translation stage that moves the fibre through the focus of a femtosecond laser. Using the PbP technique, the gratings are typically written using relatively high laser pulse energies (~100 nJ in silica fibre) which results in the formation of an array of Type-II-IR microvoids within the core of the fibre (which may lead to high level of scattering losses) and a correspondingly high refractive index contrast (see Figure 4.2) [9, 37, 54]. In 2013, Hudson *et al* demonstrated a single longitudinal mode fibre laser operating at 2914 nm in which the narrow linewidth feedback was provided by an FBG that was directly inscribed into the Ho^{3+}-Pr^{3+} co-doped fluoride fibre using the femtosecond laser PbP inscription technique [45]. In this work, it was also shown that in contrast to silica-glass fibres, the induced modifications in ZBLAN fibres do not constitute microvoids, but relatively strong Type-I-IR modifications.

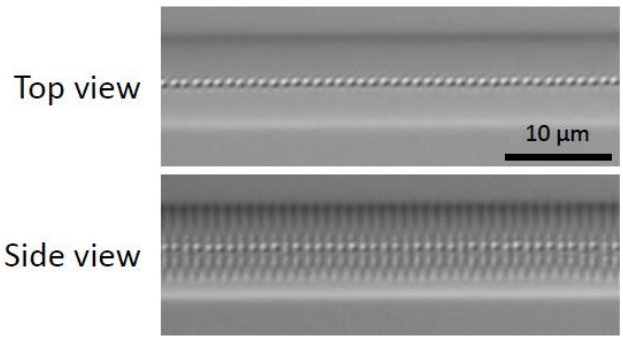

Figure 4.2: Microscopic images of a PbP grating inscribed into silica fibre viewed parallel (top) and perpendicular to the writing beam (side) [9].

4.2.2 Continuous and modified core-scanned inscription method

Alternative direct write techniques that overcome the limitations of the PbP method are the continuous and modified core-scanning inscription techniques which, in general, can lead to the formation of stronger gratings as the induced index modifications can be extended through the entire cross-section of the fibre core, even in large-mode-area (LMA) fibres [55]. Moreover, the fabrication of more complex grating geometries like CFBGs becomes feasible as has been demonstrated in the case of silica-fibres [56]. However, the need to strip off the polymer coating of the fibre before the actual FBG fabrication process remains an issue.

4.3 Inscription setup

A Ti:Sapphire femtosecond laser (Spectra-Physics Hurricane) was used to inscribe the FBGs. The laser emits pulses at a repetition rate of 1 kHz at a wavelength of 800 nm with a duration of 115 fs. The fibre used in these experiments was a silica (SMF-28e) and a Ho^{3+}-Pr^{3+} co-doped double clad ZBLAN fibre, respectively. All gratings were inscribed in mechanically/chemically stripped fibres with 125 μm cladding diameter. To ensure that the fibre was held perfectly straight during the inscription process, a custom designed V-groove was machined into a glass substrate using a picosecond laser. The fibre was then immersed in index matching oil, placed into the V-groove and subsequently covered with a 100 μm thick glass coverslip to eliminate aberrations caused by curved air-glass interfaces. This assembly was then mounted onto a programmable three-axes air-bearing translation stage, to move the

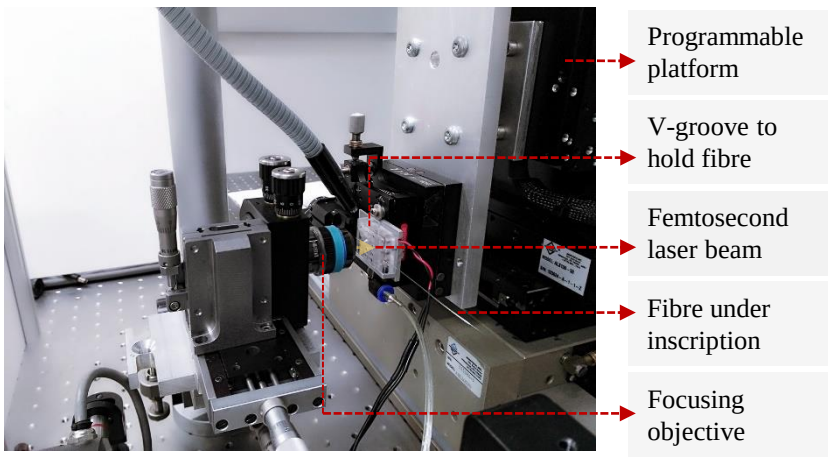

Figure 4.3: Modified core-scanned inscription setup.

fibre in a rectangular pattern transversely through the focus of the laser beam to perform the modified core scanned inscription. The amplitude of this rectangular modulation was adjusted to ensure that the induced index modification extends through the entire core of the fibre during the fabrication process. The pulse energies used for the inscription of FBGs in silica and ZBLAN fibres were 90 nJ and 150 nJ respectively. Femtosecond laser pulses were focused into the core of the optical fibre using a 20x oil-immersion objective with an NA of 0.8 (Olympus) which resulted in the formation of tracks of Type-I modifications within the fibre. Figure 4.3 shows the modified core-scanned inscription setup which consists of an Aerotech FA 130 US translation stage that controls the movement across the transverse axes and an Aerotech ABL 2000 stage for movement parallel to the fibre axis [56]. The total length of the inscribed gratings was between 10–15 mm.

4.4 Experimental results and discussions

This section presents the experimental results and discussions of FBGs fabricated in stripped silica and active ZBLAN fibres using the core-scanned method.

4.4.1 Uniform and chirped FBG inscription in silica fibres

All uniform gratings in silica fibres were fabricated with a Bragg wavelength close to 1550 nm with the aim to establish the fabrication method and to simplify the characterization. The reflectivity spectra were measured using a swept wavelength system (JDSU SWS 15100),

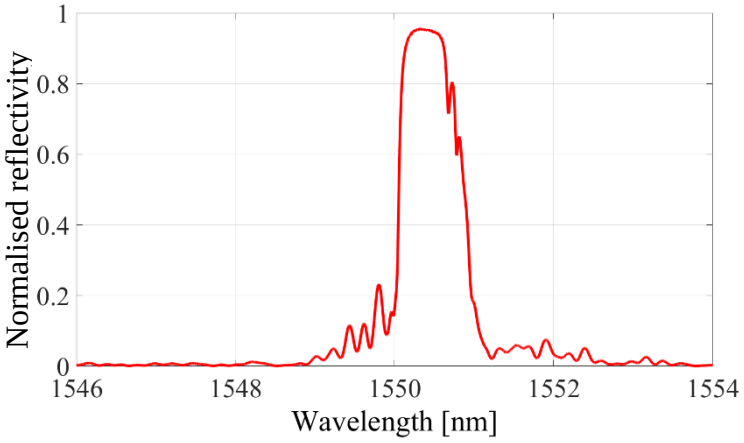

Figure 4.4: Reflection spectrum of a 10 mm long core-scanned uniform grating written close to 1550 nm.

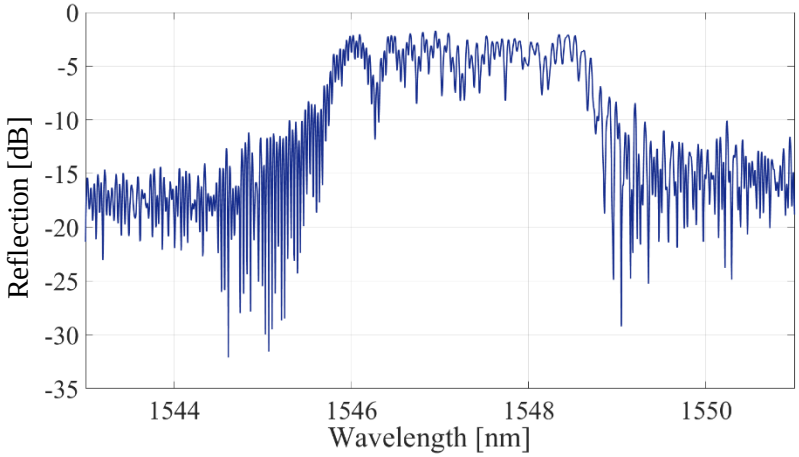

Figure 4.5: Reflection spectrum of a 15 mm long core-scanned chirped grating centered at 1547 nm.

which covers the telecom C-band (1520–1570 nm). Figure 4.4 shows the reflection spectrum of a 10 mm long uniform FBG inscribed using the core-scanned method. The observed reflectivity was 96% with a bandwidth of ~0.7 nm.

Next, a linearly chirped grating of physical length 15 mm was also fabricated using the core-scanned method. Figure 4.5 shows the reflection spectrum of a CFBG with a bandwidth of 3 nm spanning from 1546–1549 nm and a reflectivity of ~40%. For Corning SMF-28e fibre with a refractive index n=1.468 at 1550 nm and a grating length of L=15 mm, the total group delay can be calculated as $t = \frac{2Ln}{c}$=147 ps [14]. From the datasheet of SMF-28e fibre it can be noted that the dispersion at a signal wavelength of 1550 nm is ~17 ps/nm.km. This suggests that the CFBG inscribed over 15 mm length could be used to compensate the dispersion of approximately 3 km of standard single mode fibre.

4.4.2 Uniform FBG inscription in active ZBLAN fibres

In comparison to silica fibres, the transmission and reflection spectra measurements of uniform gratings written in ZBLAN fibres at mid-IR wavelength are more complicated due to the lack of an appropriate broadband characterisation source. In order to evaluate the strength of FBGs inscribed into stripped ZBLAN fibres, several gratings were inscribed into the core of sections of Ho^{3+}-Pr^{3+} co-doped ZBLAN fibres and a high-power multi-mode 1150 nm laser diode was used to pump the active fibre. However, the chemical stripping process made the fibre weak and fragile making it difficult to work with. Note that ZBLAN is a much softer glass compared to fused silica. The lasing peaks observed at various wavelengths are

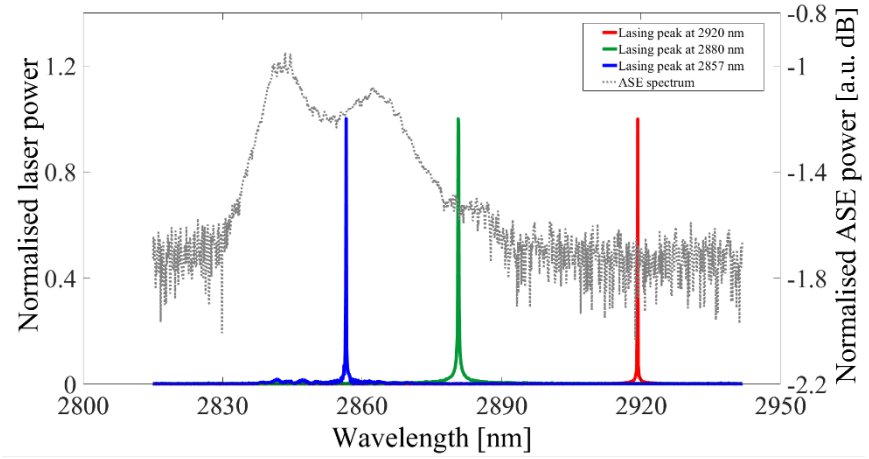

Figure 4.6: Lasing spectrum obtained from various FBGs written in active ZBLAN fibre.

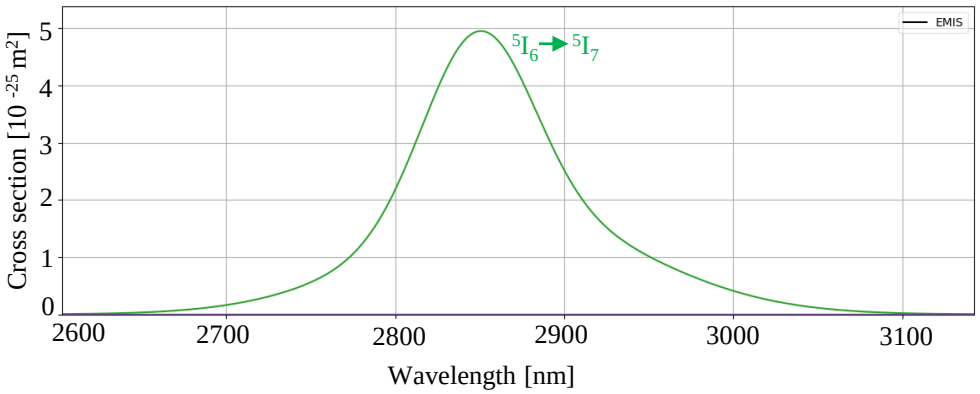

Figure 4.7: Emission cross section of Ho^{3+} ions when pumped with 1150 nm laser diodes.

shown in Figure 4.6. FBG fabrication in active ZBLAN fibre at wavelengths >2940 nm did not result in lasing at that wavelength. This could be due to the small emission cross section of Ho^{3+} ions at this wavelength as shown in Figure 4.7. In fact, the emission cross section beyond 2950 nm is more than an order of magnitude lower than at its peak at a wavelength around 2850 nm.

4.5 Mechanically robust ZBLAN fibre Bragg grating

In this section, we report on the inscription of a mechanically robust FBG into a 480 µm wide double-clad active ZBLAN fibre in a simple one-step process that neither requires a phase mask nor the removal of the polymer jacket of the fibre. To the best of our knowledge, this is the first demonstration of the inscription of a mechanically strong FBG through the polymer coating of a doped double-clad fluoride fiber without using a phase mask. This robust fabrication method helped us to improve the strength of the grating, made it easier to handle and avoided stripping the jacket since this may cause scattering of pump light from

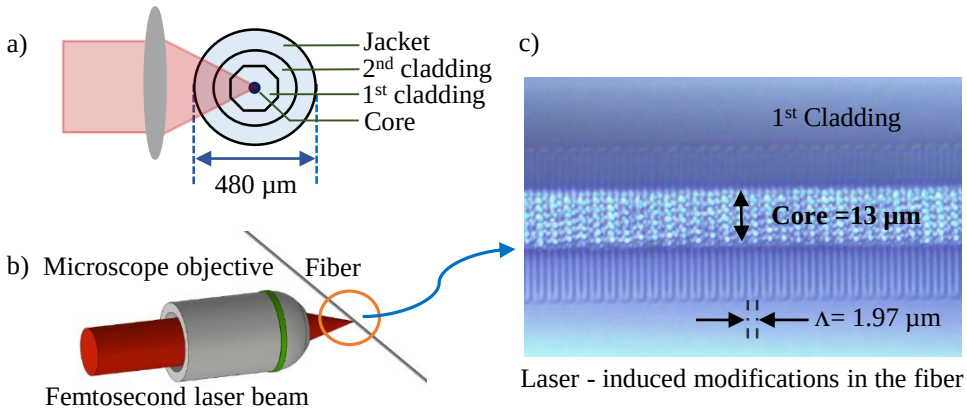

Figure 4.8: (a) Cross-sectional view of the active fiber and schematic representation of the process of focusing the inscription laser into its core. (b) Femtosecond laser direct write setup and (c) a microscopic image of the FBG.

the first cladding of the double-clad fibre.

4.5.1 Fabrication method

The inscription methodology is basically the same as described in Section 4.3. However, the fibre used in the experiments was a Ho^{3+}-Pr^{3+} co-doped double clad ZBLAN fibre with a core diameter of 13 µm and in contrast to all previous experiments, the fibre jacket was not stripped off before grating inscription. The octagonal shaped first cladding had a diagonal length of 125 µm and the outer cladding diameter of 210 µm was surrounded by an acrylic jacket of 480 µm as schematically shown in Figure 4.8(a). A V-groove was specially machined to hold the fibre during inscription. Femtosecond laser pulses with an energy of 270 nJ were tightly focused into the core of the optical fibre through the 480 µm polymer coating using a 40x dry-objective with an NA of 0.6 (Olympus) which resulted in the formation of tracks of Type-I modifications within the core of the fibre. Given the large diameter of the active double-clad fiber, the laser intensity at the polymer coating (520 kW/m^2) is almost three orders of magnitude lower than the laser intensity at the core (380 MW/m^2). Therefore, the laser intensity levels used in our experiments will not damage the fiber coating under no circumstances. Figure 4.8(b) depicts a schematic representation of the fabrication process and Figure 4.8(c) shows a differential interference contrast (DIC) microscopic image of the femtosecond laser inscribed highly uniform pattern within the core of the fibre. The physical length of the inscribed second-order grating was 15 mm (grating period = 1.97 µm). Note that a second-order grating was chosen as to avoid overlap between adjacent grating planes

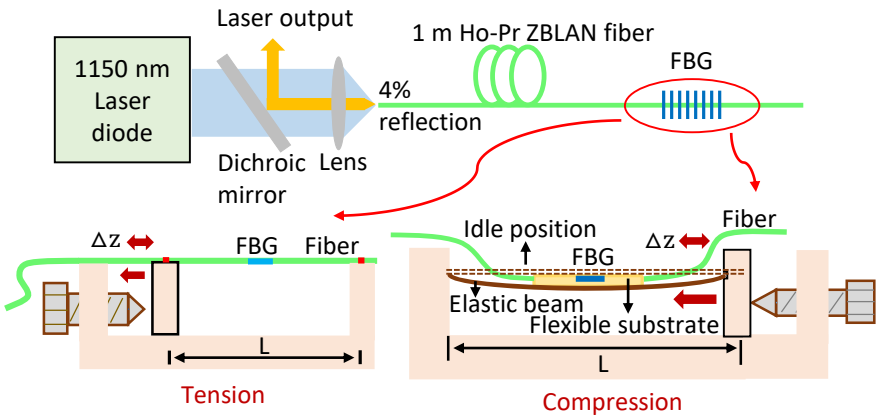

Figure 4.9: Experimental setup for tension and compression tuning of the FBG.

while maximizing the grating strength for a given length. The total time required to inscribe the gratings was approximately 2 hours.

4.5.2 Widely tunable all-fibre mid-IR laser using a mechanically robust FBG

This section details the development of a widely tunable all-fibre mid-infrared laser system based on a mechanically robust FBG which was inscribed through the polymer jacket of an active fluoride fibre by focusing femtosecond laser pulses into the core of the fibre without the use of a phase mask.

The tunable fibre laser consisted of a 1 m long section of double-clad ZBLAN fibre, co-doped with Ho^{3+} and Pr^{3+} rare-earth ions (molar concentration of 35000:2500 ppm) and is depicted schematically in Figure 4.9. A high-power multi-mode 1150 nm laser diode was used to pump the active fibre and a CaF_2 lens with a focal length of 20 mm (anti-reflection coated for 2900 nm) focused the pump beam into the fibre. In-between the laser diode and the pump coupling lens, a dichroic mirror with high reflectivity (98%) at the laser wavelength and high transmission (96%) at the pump wavelength was used to split the pump and signal wavelengths. The input end of the fibre was perpendicularly cleaved, and the 4% Fresnel reflection acted as a low reflectivity broadband mirror while feedback from the high reflectivity FBG (~ 50%) at the other end completed the Fabry-Perot laser cavity. This reflectivity value suggests that the induced refractive index contrast is approximately $1{\times}10^{-4}$ [72]. Previous studies demonstrate that the reflectivity of the FBG could be increased further if required, by optimizing the parameter of the direct write procedure [55, 73]. Without

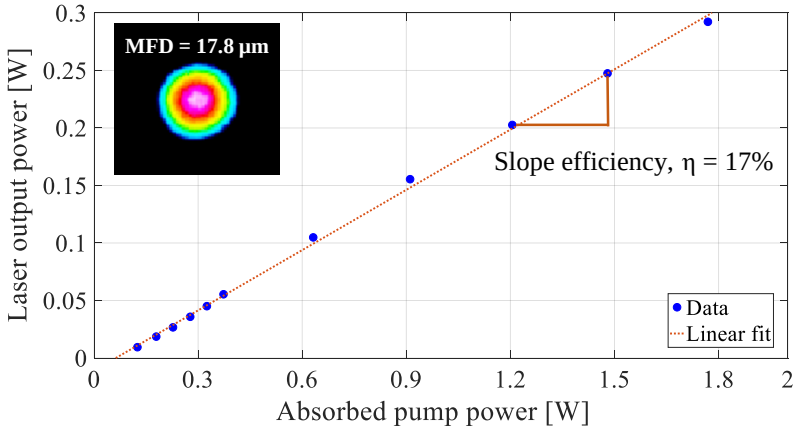

Figure 4.10: Laser slope efficiency with respect to absorbed pump power. The inset shows the laser beam profile.

applying any tension or compression to the FBG, the laser spectrum was initially centered at 2880 nm and had a line width of 105 pm which was close to the resoultion of the optical spectrum analyser (100 pm). Thus, the measured line width of the laser could be limited by the resolution of the spectrum analyzer. In Figure 4.10, the output power of the laser with respect to absorbed pump power is shown, indicating a slope efficiency of 17% and a threshold of 66 mW. The efficiency could be improved further by using a longer length of the active fibre and/or by inscribing a broadband (chirped) grating at the input end of the fibre with a reflectivity larger than the 4% provided by Fresnel reflection, see section 4.5.3. Figure 4.10 inset shows an image of the laser beam profile having a mode-field diameter (MFD) of 17.8 µm, which indicates the absence of any transverse modes other than the fundamental LP_{01} mode.

Applying tension or compression to the FBG changes the effective period Λ of the grating and thus its Bragg wavelength ($\lambda_B = 2\Lambda n_{\text{eff}}$, where n_{eff} is the effective index of refraction of the core mode). The deformation in the grating period is proportional to the amplitude of the perturbation force and this results in tuning of the lasing wavelength. However, the tuning of the lasing wavelength by applying tension or compression is limited by the mechanical strength of the fibre since it is susceptible to fracture under even moderate tensile forces if any microvoids, scratches or cracks are present.

To mechanically stretch the FBG for wavelength tuning, we fixed one end of the grating while the other end was glued to a linear translation stage using a fast-drying epoxy as shown in Figure 4.9. When axial tension was applied to the FBG by adjusting the micrometer

screw, the associated mechanical stretching of the fibre produced a linear red-shift of the laser wavelength of 1.29 nm/millistrain (m$\epsilon = \frac{\Delta z}{L} \times 10^3$). The tensile tuning range was limited to 7 nm as the optical fibre experienced structural failure beyond 31.29 N. This applied tension was estimated by assuming Young's modulus of ZBLAN glass as 53 GPa [57]. As a comparison, we also performed tensile tuning tests under identical conditions but using a fibre that was stripped of its polymer jacket before FBG inscription. In this case, the observation reveals the fibre stress fracture limit is enhanced by 62% when the inscription is performed through the polymer jacket compared to a stripped fibre, making this inscription method more robust and promising for practical devices. The fibre strength limitations related to tension tuning are considerably relaxed if a compression force is applied as the compressive strength of materials is generally higher than their tensile strength [58]. For compression measurements, it is essential to compress the fibre strictly along its axis to avoid buckling.

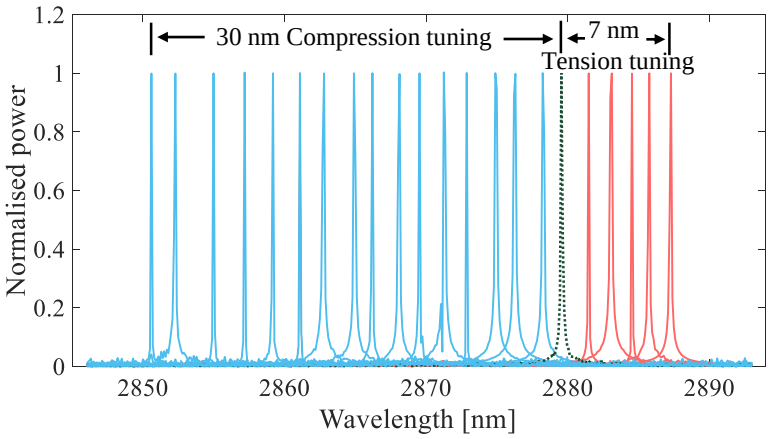

Figure 4.11: Spectra of the shifted laser output peaks.

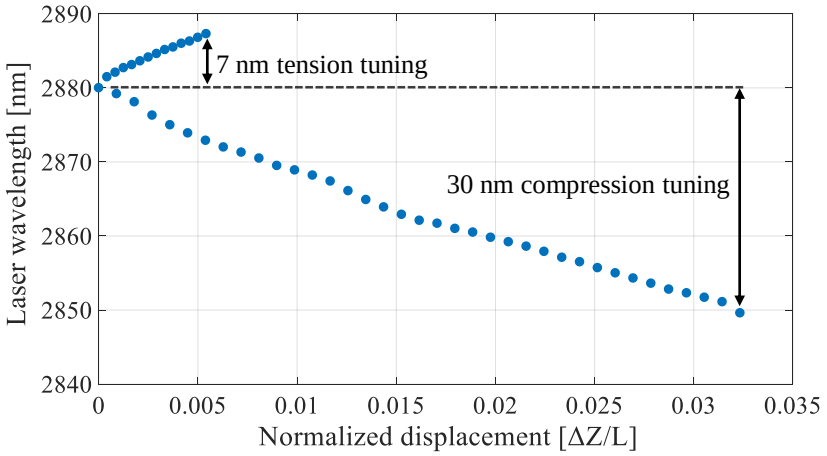

Figure 4.12: Measured tuning range of the tunable laser source.

The fibre section containing the FBG was therefore fixed to an elastic steel beam of length L = 16.5 cm, width W = 1.2 cm and thickness H = 0.1 cm. This steel beam was placed in-between a fixed stage and a movable translation stage that was controlled by a micrometer screw [59]. To prevent vertical movement and buckling of the fibre during tuning, the FBG was secured within a flexible substrate (thickness $D \sim 4$ mm) having a low Young modulus of 1.03 GPa. Upon curing, the substrate adheres to the elastic steel beam which has a high Young's modulus of 180 GPa. Note that utmost care was taken to avoid micro-bubbles inside the flexible substrate during the curing process as adverse effects could otherwise result in the micro-bending of the fibre while tuning. The inward translation of the movable block deformed the beam into an arc shape, where the displacement of the movable block Δz, normalized by the length of the beam L, is related to the arc angle θ by [60],

$$\frac{\Delta z}{L} = \left[1 - \frac{sin(\theta/2)}{(\theta/2)}\right]. \tag{4.2}$$

The arc angle θ in Eqn. 4.2 can be calculated by measuring the displacement of the micrometer screw and the length of the elastic beam. Therefore the strain applied to the FBG is [60],

$$\epsilon = \frac{\theta D}{L}. \tag{4.3}$$

The maximum strain applied to the FBG embedded in the flexible substrate before failure was estimated from Eqn. 4.3 to be 21.57 mϵ.

As shown in Figure 4.11, compression measurements indicate a maximum blue-shift of the laser wavelength of 30 nm. This is equivalent to a tuning range that is more than 4 times larger compared to the tuning range achieved by stretch-tuning, because of the higher compression strength of the ZBLAN fibre over its tensile strength. The laser linewidth across the entire tuning range was less than 112 pm. Figure 4.12 illustrates the wavelength shift of the CW laser with respect to the displacement of the micrometer screw, normalized to the length of the beam, demonstrating continuous tunability from 2850 nm to 2887 nm.

In conclusion, to the best of the author's knowledge, this is the first demonstration of the fabrication of a mechanically strong FBG through the polymer coating of an active double-clad fluoride fibre without using a phase mask. A stable, 37 nm wavelength tunable FBG-based narrow-linewidth continuous wave fibre laser was demonstrated by applying tension and compression to the FBG and this is the first time wavelength tuning of a fibre laser has been demonstrated with FBGs written in ZBLAN fibre. This demonstration paves

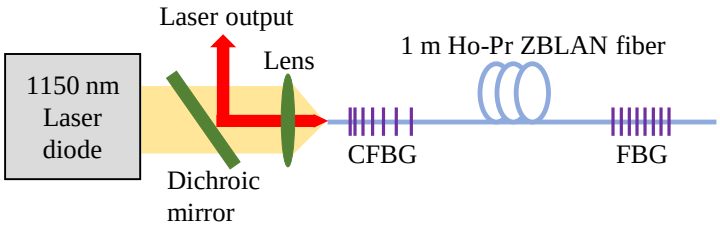

Figure 4.13: Fabry-Perot laser cavity with CFBG and FBG.

the way to the development of robust, narrow-linewidth, all-fibre mid-IR lasers for practical applications outside the laboratory.

4.5.3 Fabry-Perot laser cavity with increased efficiency

As mentioned in the previous section, the efficiency of the Fabry-Perot laser cavity with only one FBG and 4% Fresnal reflection can be further improved by inscribing a CFBG into the core of the active fibre at the input end which effectively enhances the Q-factor of the cavity.

The schematic representation of the experimental setup is illustrated in Figure 4.13. The

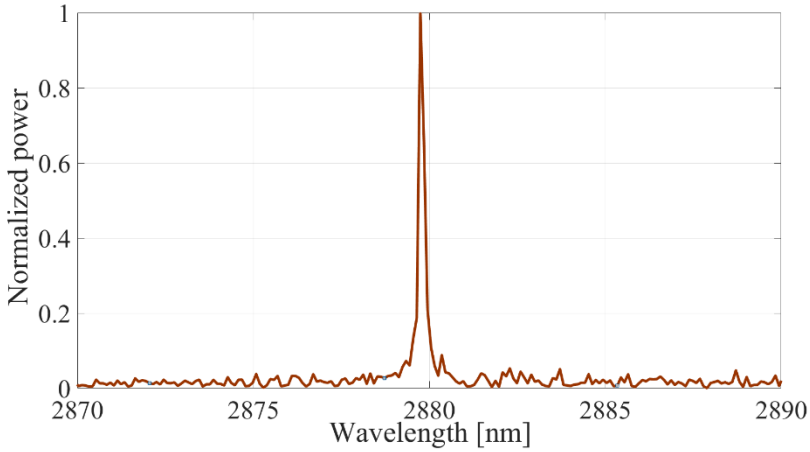

Figure 4.14: Optical spectrum of the Fabry-Perot laser.

laser cavity consists of a 1 m long section of active ZBLAN fibre confined by two FBGs. One side of the cavity has a uniform FBG (2880 nm) of narrow bandwidth of ~ 0.1 nm and the other end has a CFBG which has a reflective bandwidth of 1 nm (2879.5–2880.5 nm) which ensures its spectral overlap with the output FBG. Both FBGs were fabricated using the direct write technique with 800 nm femtosecond laser pulses for 15 mm physical length. A mid-IR optical spectrum analyser was used to characterize the spectrum of the laser which is shown in Figure 4.14 with a full width at half maximum (FWHM) bandwidth of <108 pm.

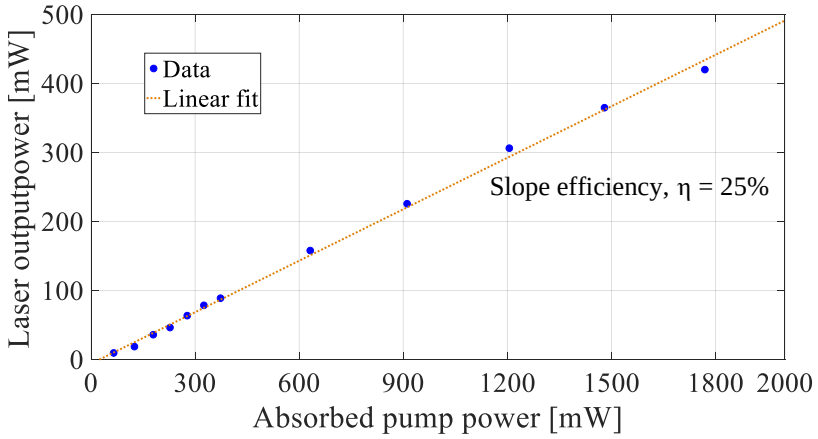

Figure 4.15: Slope efficiency of the Fabry-Perot laser cavity with two FBGs .

Compared to before, the slope efficiency was improved from 17% to 25% with a maximum output power of 0.42 W at a wavelength of ~ 2880 nm (see Figure 4.15). The current slope efficiency is 62.5% of the Stokes efficiency limit. However, this slope efficiency could be further improved by using a longer length of fibre.

4.6 Chapter summary

In this chapter, various inscription methods of fibre Bragg grating in silica and ZBLAN fibres have been detailed. Most importantly, the fabrication of mechanically robust FBGs in active ZBLAN fibres without the use of a phasemask was demonstrated. Using this FBG, a widely tunable all-fibre mid-infrared laser system was developed by applying mechanical tension and compression to the FBG while pumping the fibre with an 1150 nm laser diode. A continuous wave all-fibre laser with a tuning range of 37 nm, centered at 2.87 μm was demonstrated with up to 0.29 W of output power. Later, the slope efficiency of this laser was further improved to 25% by inscribing an additional CFBG into the laser cavity. These results pave the way for the realisation of compact and robust mid-infrared fibre laser systems for real-world applications in spectroscopy and medicine.

5

Integrated Optical Components

The fundamental advantage of a monolithic (all-fibre) approach is the absence of any free space bulk optical components which greatly increases the robustness and compactness of a laser and reduces its cavity losses. As there is also no need for careful optical alignment, such systems lend themselves operation by non-expert users. The availability of integrated photonic components such as splitters, couplers, X and Y junctions would be an important advancement in mid-IR fibre laser technology as those can be effectively used to replace all bulk optical elements in a fibre ring laser cavity which is the preferred geometry for the generation of ultrashort laser pulses.

The prerequisite is that these integrated components have minimized losses which include mode-field diameter (MFD) and numerical aperture (NA) mismatch losses as well as Fresnel, propagation and bend losses [11]. Such low-loss integrated optical components are believed to become the main building blocks for future all-fibre laser systems in the mid-IR region. The material selected for fabricating these devices must be transparent in the mid-IR and also compatible with the ultra-fast laser inscription technique. ZBLAN and chalcogenide glasses

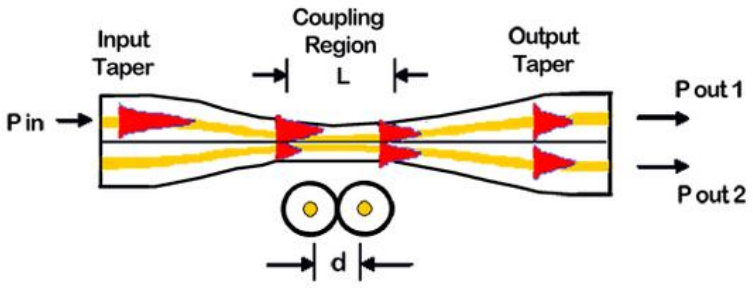

Figure 5.1: Principle of operation of an optical coupler using evanescent wave coupling [10].

are two promising candidates meeting these requirements [61]. This chapter outlines the comparison of experimental results of optical couplers inscribed in both glasses for operation at near and mid-IR wavelengths. These couplers were initially fabricated to operate at 4 μm and 3.4 μm, respectively. However, the purpose of this chapter is to investigate the the feasibility of using these optical couplers in future fully integrated mid-IR laser systems operating at 2.9 μm.

5.1 Optical couplers

An optical directional coupler splits light injected into one input port to one or more output ports, often through evanescent wave coupling. The optical coupler can be formed by fusing fibres together or using chips (polished glass substrates), which is the method we use in our experiments. The intensity profile of the light traveling down the core of a coupler is typically Gaussian like. That means, the intensity is maximum at the center and tapers off as the core/cladding interface is approached. The tail ends (called the evanescent wave) of the Gaussian profile can extend into a near by second waveguide and this allows for an exchange of energy as illustrated in Figure 5.1 (evanescent wave coupling) [10]. The amount of energy exchange depends on the wavelength of input light, the proximity of the two cores (d) and the length (L) over which this exchange takes place (coupling region). By selecting the proper length, any given power transfer ratio can be realized [10]. Besides, it can also act as a wavelength division multiplexer (WDM) to couple pump light into a laser cavity and as an output coupler in lasers for splitting off a fraction of light of a particular wavelength. A proposed integrated ring laser setup contains a directional coupler fabricated into ZBLAN or chalcogenide glass and is depicted in Figure 5.2. In the following sections, we will examine and compare the characteristics of couplers inscribed into ZBLAN and chalcogenide glasses.

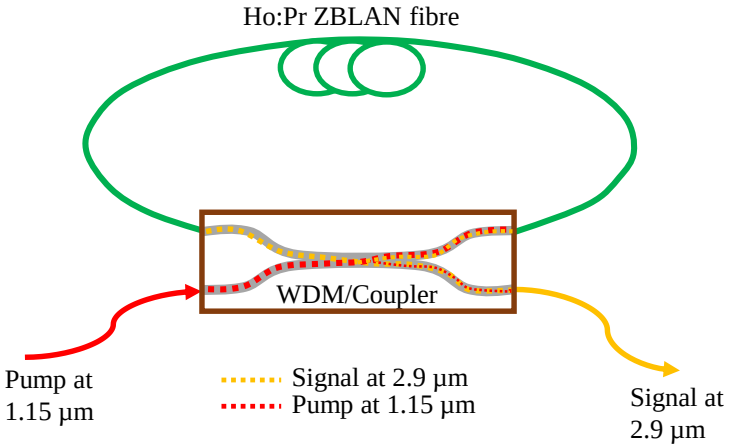

Figure 5.2: Schematic of the proposed fully fibre integrated ring laser setup using a directional coupler.

5.2 Optical coupler inscribed into ZBLAN glass

Waveguide Bragg gratings and waveguide lasers were demonstrated around 2 µm wavelength region in ZBLAN glass utilising the femtosecond laser direct-write technique [62, 63]. In contrast to fused silica and quartz, ZBLAN exhibits negative index change when irradiated by femtosecond laser pulses [11, 64]. Hence, the modified region can be used as the cladding of a waveguide. Thus, waveguides in ZBLAN are typically fabricated by stitching multiple

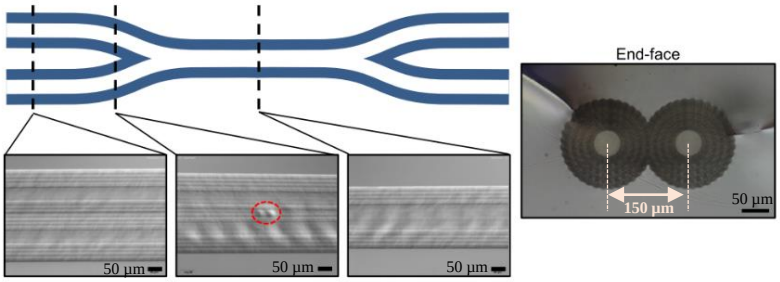

Figure 5.3: Schematic of the depressed cladding directional coupler with transmission differential interference contrast microscope images taken at different positions of the device. The red circle indicates defects created by hard on/off switching of the femtosecond laser. An image of the end facet of the directional coupler is shown on the right-hand side. Stress-fractures are apparent at the edges of the cladding, however without affecting the waveguide performance [11].

tracks together to form a depressed cladding [11]. This method offers great flexibility to form waveguides of arbitrary core size and cladding thickness by simply adding more tracks, making it suitable for long wavelength operation [11].

5.2.1 Fabrication of directional couplers into ZBLAN glass

The ZBLAN glass used in our experiments was fabricated in a controlled atmosphere glass melting facility to cast 50 g glass ingots, at the University of Adelaide [11]. In order to fabricate the directional couplers, the ingot was sliced using a CNC diamond saw into several chips of 39 mm length, 12 mm width and 3 mm height. Later, the top and bottom faces of each sample were polished to permit the femtosecond laser inscription. The couplers were inscribed by Gross *et al* in our labs using the high repetition rate femtosecond laser direct write technique (discussed in Chapter 3) since the exposure area required for a depressed cladding waveguide is larger than a single line waveguide. The pulses from a Ti:sapphire oscillator (FEMTOSOURCE XL 500) with 800 nm center wavelength, <50 fs pulse duration and 5.1 MHz repetition rate were focused into the sample using a 1.25 NA, 100× oil immersion objective. The sample was translated transversely through the focus of the femtosecond laser beam using a three-axis air-bearing translation stage. The pulse energy used to inscribe those couplers was 65 nJ [11]. The depressed cladding directional couplers were inscribed with 50 μm core diameter and 60 μm cladding thickness. The total length of the device was 33.6 mm. The estimated refractive index contrast of the waveguide is $\Delta n=7\times10^{-4}$ resulting in an NA of 0.046 [11]. The input and output ports of the directional coupler were separated by a distance of 150 μm. The schematic of the directional coupler is depicted in Figure 5.3 which includes microscope images taken at different sections of the device showing transition from two individual waveguide cores to a single large core in the coupling region. To create the coupling region, the laser was switched off once the modification would cross the middle plane of the device [11]. The encircled portion in Figure 5.3 indicates the minor defects occurred at the ends of the individual modifications due to switching the laser on and off. These defects can be a source of additional loss but can be avoided by smoothly changing the laser power [11].

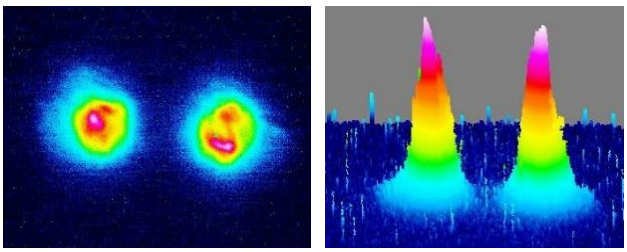

Figure 5.4: Image of the output facet of the directional coupler at 1.15 μm wavelength.

5.2.2 Characterization of directional couplers fabricated in ZBLAN glass

The ZBLAN optical coupler was initially designed and fabricated by Gross *et al* for astronomic applications at 4 μm wavelengths [11]. However, in this work it was characterized at 1.15 μm pump wavelength as well as 2.9 μm emission wavelength of Ho:Pr co-doped ZBLAN fibre in order to investigate its suitability as a coupler/WDM in a ring laser cavity.

Characterization at 1.15 μm wavelength

In order to attain mid-IR emission at 2.9 μm, in Ho^{3+}:Pr^{3+} co-doped ZBLAN fibre laser, one needs to excite the $^5I_6$-$^5I_7$ transition using 1.15 μm pump photons as discussed in Section 2.2. Commercial availability of high power diode lasers at 1.15 μm (Eagleyard Photonics) aided the development of mid-IR laser system at 2.9 μm. The laser output from a 1.15 μm diode was coupled to a multi-mode silica fibre of 105 μm core diameter with 0.1 NA using a 20 mm focal length uncoated CaF_2 lens with a coupling efficiency of 73%. This fibre is the closest match available to the 50 μm core and 0.046 NA directional coupler. During the experiment, the ZBLAN chip was mounted on an XYZ translation stage for precise alignment. The fibre was butt-coupled to the chip. The output light from the chip was then focused onto a silicon-based charge coupled device (CCD) camera using a 75 mm focal length plano-convex lens. The coupler was multi-moded at the pump wavelength and Figure 5.4 indicates the presence of some higher order modes at 1.15 μm wavelength. The coupling ratio at the output of the coupler was found to be 54:46 which means 46% of the pump light would not be coupled into the doped fibre laser cavity as shown in Figure 5.2. Beyond this loss, additional losses were also estimated for the directional coupler at the pump wavelength 1.15 μm and are shown in Table 5.1. The NA mismatch was calculated as 6.72 dB using Eq.5.1 where NA_1 is the NA of the fibre, NA_2 is the NA of the coupler and $NA_1 \geq NA_2$ [65]. Likewise, the Fresnel

reflection on one interface of the chip can be estimated as 0.18 dB using Eq.5.2 where n_{glass} is the refractive index of the glass substrate (n_{ZBLAN}= 1.48 at 1.15 μm and 1.50 at 2.9 μm respectively), n_{air} is the refractive index of air (n_{air}= 1) [16]

$$NA\ mismatch\ loss\ (dB) = 10\ log\left[\frac{NA_2}{NA_1}\right]^2, \tag{5.1}$$

$$Fresnel\ reflection\ (dB) = 10\ log\left(1 - \left[\frac{n_{glass} - n_{air}}{n_{glass} + n_{air}}\right]^2\right). \tag{5.2}$$

Various losses	Loss (dB)
NA mismatch loss	6.72
Fresnel reflection loss on both sides of chip	0.36
Propagation loss (0.34 dB/cm) [11]	1.14
Total loss	8.22

Table 5.1: Various estimated losses of the ZBLAN coupler at 1.15 μm wavelength .

Characterization at 2.9 μm wavelength

The light source used to probe the directional coupler was a Fabry-Perot laser consisting of a 0.5 m long section of Ho^{3+}:Pr^{3+} co-doped ZBLAN fibre with 13 μm core diameter with 0.13 NA. The fibre was pumped by a 1.15 μm laser diode and a CaF_2 lens with a focal length of 20 mm (anti-reflection coated for 2.9 μm) focused the pump beam into the fibre. The input end of the fiber was perpendicularly cleaved, and butt-coupled to a dichroic mirror with high reflectivity (98%) at the signal wavelength and high transmissivity (99%) at the pump wavelength. The output end of the fibre was perpendicularly cleaved, and the 4% Fresnel reflection acted as a low reflectivity broadband output coupling mirror and thereby forming a Fabry-Perot cavity as depicted in Figure 5.5. The output of this linear cavity was then coupled to the directional coupler. The output light from the chip was focused onto a vanadium oxide microbolometer based camera (designed for 2–16 μm wavelength) using a 75 mm focal length plano-convex lens. A bandpass filter centered at 2.9 μm was used to filter out any unabsorbed pump light. The coupler was single moded at 2.9 μm (LP_{01}) and Figure 5.6 shows the near-field image of the output of the directional coupler observed at 2.9 μm wavelength exhibiting a coupling ratio of 18:82.

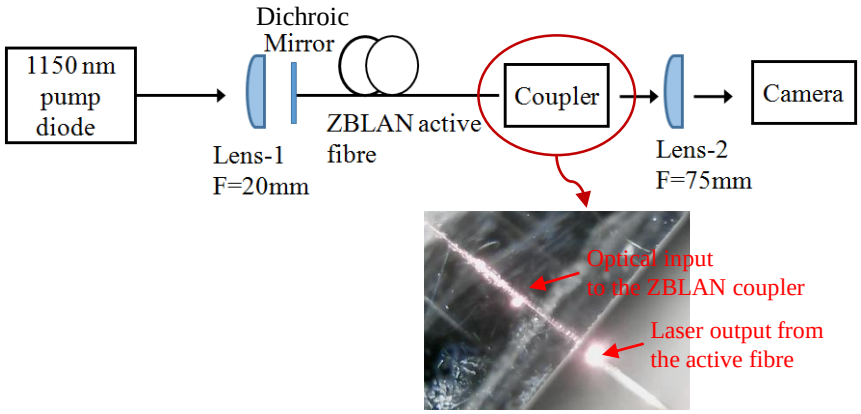

Figure 5.5: Experiment setup for the ZBLAN coupler characterization at 2.9 µm.

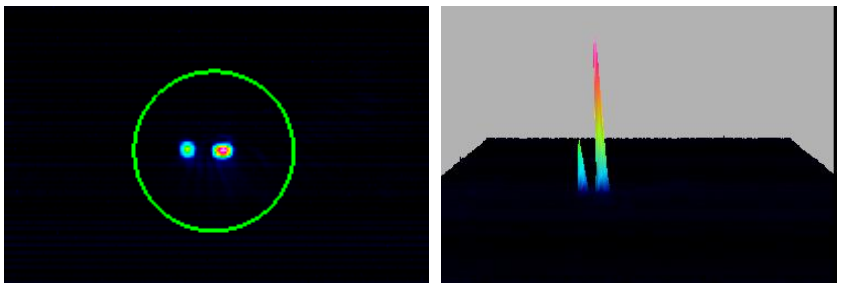

Figure 5.6: Image of the output facet of the directional coupler at 2.9 µm wavelength.

Losses were estimated for the directional coupler at 2.9 µm signal wavelength as shown in Table 5.2. The overall loss includes NA mismatch loss as well as Fresnel reflection and propagation loss in the ZBLAN coupler. Significant losses are caused by the large NA mismatch while other sources of losses are minor. Assuming a laser cavity would be formed using this ZBLAN coupler, then as a result of this NA mismatch, the cavity losses would be excessive at each round trip. Thus, very high pump power levels would be required to produce sufficient gain in the laser cavity to overcome these losses which is highly impractical. In

Various losses	Loss (dB)
NA mismatch loss	9.02
Fresnel reflection loss on both sides of chip	0.36
Propagation loss (0.29 dB/cm) [11]	0.97
Total loss	10.35

Table 5.2: Various estimated losses of ZBLAN coupler at signal wavelength 2.9 µm.

addition to that, it is impossible to improve the NA of the coupler further as it has been shown that the change in refractive index cannot be considerably modified in ZBLAN [6], thus the NA mismatch loss is inevitable in ZBLAN couplers. Hence, our conclusion is that ZBLAN couplers are not suited to realise a fully integrated ring laser cavity.

5.3 Optical coupler inscribed into chalcogenide glass

Early work on femtosecond laser inscription in chalcogenide glasses started with arsenic selenides (As_2Se_3) [66] and arsenic sulphides (As_2S_3) [67]. Like ZBLAN, these glasses exhibit a negative refractive index change when exposed to a femtosecond laser. The inclusion of Germanium to form Ge-As-S glasses has been shown to have an effect on the sign and magnitude of the refractive index change generated during ultrafast laser inscription [68]. Replacing arsenic with gallium leads to a highly stable and non-toxic chalcogenide glass called Gallium Lanthanum Sulphide (GLS) [69]. This family of chalcogenide glasses is a promising host material for the mid-IR due to its excellent optical transparency from the near to the mid-IR (0.6–10 µm). The fabrication of low-loss single mode waveguides and couplers in the near and mid-infrared in GLS using femtosecond lasers was demonstrated by Gretzinger et al [47]. The propagation loss reported in GLS [47] was higher when compared to the propagation loss in ZBLAN [11]. However, the refractive index variation between the core and cladding is much stronger in GLS compared to ZBLAN. This may lead to an improvement in the confinement of light inside the waveguide as well as in a reduction in NA mismatch loss when compared to the couplers fabricated in ZBLAN.

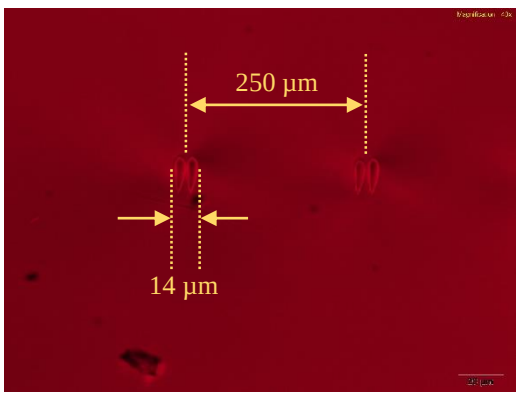

Figure 5.7: End on view of the inscribed couplers in GLS using 11 nJ pulse energy.

5.3.1 Fabrication of the directional coupler into GLS glass

The GLS glass samples for the inscription of directional couplers were obtained from the Chalcogenide Advanced Manufacturing Partnership of the University of Southampton (ChAMP), and had a dimension of $25 \times 25 \times 1$ mm with all sides polished. In the cumulative heating regime (as discussed in chapter 3), a high repetition rate (5.1 MHz) Ti: sapphire chirped pulse femtosecond oscillator (Femtosource XL500, Femtolasers GmbH) with high pulse intensities induced local melting of the glass, thereby forming refractive index modifications in the GLS sample [70]. The laser emits up to 550 nJ pulses at an 800 nm wavelength with a pulse duration of <50 fs [70]. A 100× oil immersion microscopic objective with 1.25 NA was used for inscription. When compared to a dry objective, the oil immersion objective reduces the spherical aberrations due to the refractive index mismatch. Gretzinger *et al* inscribed the waveguides into the GLS samples by mounting it on a programmable Aerotech air-bearing stage. In the cumulative heating regime, the thermal energy around the focal spot can cause a refractive index change with a teardrop-like cross section [47] which eventually leads to an elliptical beam profile. Because of the large observed ellipticity of the modifications in GLS, the couplers were formed by inscribing two waveguide structures next to each other [70] as shown in Figure 5.7. This helps in obtaining circular confined modes at longer wavelengths [70]. The pulse energy used for the inscription was 11 nJ. The core diameter of the inscribed coupler was 14 μm with an NA of 0.17. The input and output ports of the directional coupler were separated by 250 μm.

5.3.2 Characterization of the optical coupler fabricated in GLS glass

The directional coupler fabricated in GLS was designed for low loss operation at 3.4 μm [70]. However, the characterization of the coupler was performed at 1.15 μm pump wavelength as well as 2.9 μm signal wavelength in order to investigate its feasibility to use as a coupler/WDM in a Ho^{3+}-Pr^{3+} doped fibre based ring laser cavity.

Characterization at 1.15 μm wavelength

The laser output from a 1.15 μm diode was coupled into a silica fibre of 25 μm core diameter with 0.1 NA using a 20 mm focal length uncoated CaF_2 lens. The output light from the coupler was focused onto a silicon-based CCD camera (designed for 1.13–1.68 μm wavelength) using a 75 mm focal length plano-convex lens. The coupler turned out to be single moded (LP_{01}) at the pump wavelength as illustrated in Figure 5.8(a). The coupling ratio obtained at the output

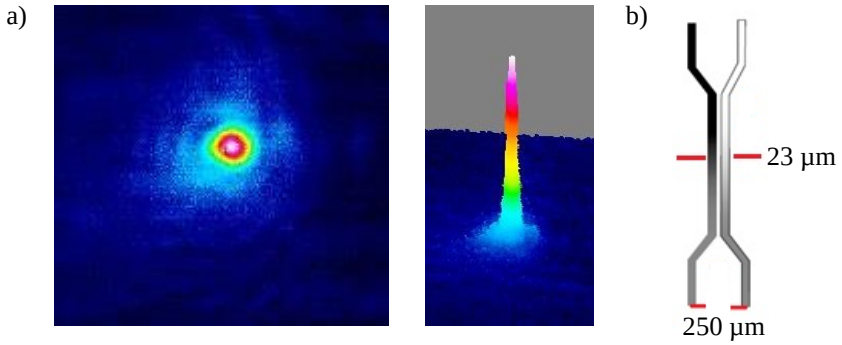

Figure 5.8: (a) Image of the output facet of the GLS directional coupler at 1.15 µm wavelength. (b) Schematic of the GLS coupler.

Various losses	Loss (dB)
MFD mismatch loss	0.11
Fresnel reflection loss on both sides of chip (~34%)	1.80
Propagation loss (1.31 dB/cm) [11]	3.27
Total loss	5.18

Table 5.3: Various estimated losses of GLS coupler at pump wavelength 1.15 µm.

of the coupler at the pump wavelength was found to be 100:0 that means no cross-coupling was observed at output port 2 compared to port 1. This can be explained by the fact that the waveguide separation in the coupling region was 23 µm as shown in Figure 5.8(b) which is not close enough for efficient evanescent wave coupling between the ports of the coupler at 1.15 µm. Various losses for the directional coupler at the pump wavelength 1.15 µm are shown in Table 5.3. The propagation loss (3.27 dB) was significant in the case of the GLS coupler when compared to that of ZBLAN coupler. However, in the case of GLS coupler, the NA mismatch loss is negligible because the NA of fibre (0.1) is smaller than that of the coupler (0.17). Instead, the mode-field diameter (MFD) mismatch loss was estimated as 0.11 dB. Fresnel reflection on the chip interface can again be estimated as 1.80 dB using Eq.5.2 where n_{GLS}= 2.38 at 1.15 µm and 2.29 at 2.9 µm respectively, n_{air}= 1.

Characterization at 2.9 µm wavelength

As in the case of the ZBLAN coupler, the light source used to probe the directional coupler was a Fabry-Perot laser consisting of a 0.5 m long section of Ho^{3+}:Pr^{3+} co-doped ZBLAN

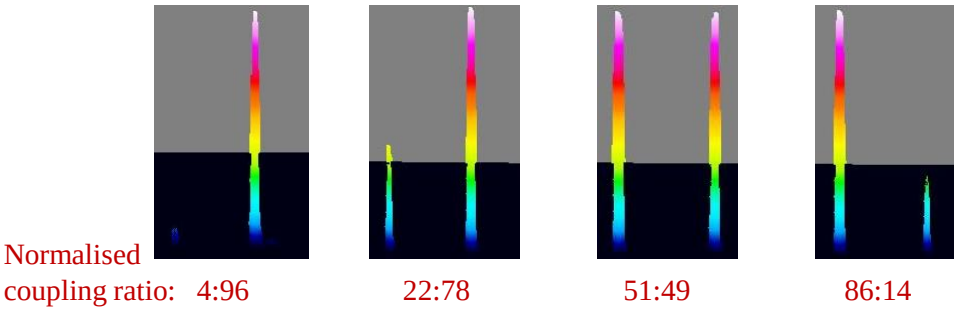

Figure 5.9: Image of the output facet of the directional coupler at 2.9 μm wavelength.

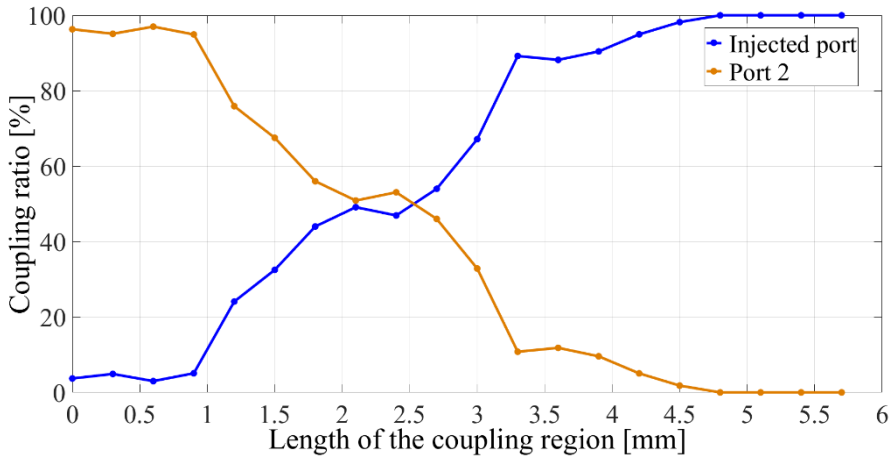

Figure 5.10: Variation in coupling ratio with respect to the length of the coupling region.

fibre. The experimental setup was the same as the setup used for characterizing the ZBLAN coupler as depicted in Figure 5.5. The GLS sample had 20 individual couplers inscribed with a varying coupling region from zero to 6 mm with a step size of 0.3 mm. Each coupler was characterized for 2.9 μm wavelength. All couplers remained single-moded throughout the measurements. However, the coupling ratio varied as per the change in the length of the coupling region. Figure 5.9 shows the images of the output facet of different directional couplers as well as the obtained coupling ratio at 2.9 μm wavelength. Figure 5.10 depicts the variation in coupling ratio of the directional couplers with respect to the length of the coupling region. The losses in the directional coupler at 2.9 μm wavelength are shown in Table 5.4. It can be seen from Tables 5.3 and 5.4 that the loss experienced at the pump as well as signal wavelengths are significantly reduced in a GLS coupler compared to a ZBLAN coupler. Propagation losses could be further reduced by optimising the glass manufacturing process and by fine tuning the inscription parameters. Our research indicates that GLS is a

Various losses	Loss (dB)
MFD mismatch loss	0.12
Fresnel reflection loss on both sides of chip (~31%)	1.60
Propagation loss (1 dB/cm) [11]	2.50
Total loss	4.22

Table 5.4: Various estimated losses of GLS coupler at signal wavelength 2.9 μm.

very promising candidate for use in mid-IR fibre ring laser cavities but further investigations are required.

5.4 Chapter summary

In this chapter, a comprehensive study on the feasibility of directional couplers inscribed in ZBLAN and chalcogenide (GLS) glass samples using ultrafast lasers for mid-IR fibre ring laser cavities was performed. In this study, various losses which can occur due to the NA mismatch, MFD mismatch, Fresnel reflection and propagation losses were analysed and measured at 1.15 μm and 2.9 μm. The couplers inscribed in ZBLAN experience significant losses at both pump and signal wavelengths, which confirms that this glass is not suitable for integration into a fibre ring laser cavity. However, from our experiments it was also observed that the performance of GLS couplers is much better when compared to ZBLAN couplers. In the future, the loss due to Fresnal reflection in the GLS coupler could be reduced by using an index matching oil or anti-reflection coating. The propagation loss could be scaled down by reducing the length of the chip or improved fabrication procedures. In addition to that, the MFD mismatch loss could be further reduced by slightly varying the diameter of the waveguides and/or by selecting better matched fibre. Hence, from our investigations, one can conclude that GLS couplers could be a promising candidate to form a fully fibre integrated ring laser cavity in the mid-IR region.

6

Conclusion

In summary, the topic of this thesis was the development of mid-IR all-fibre laser systems by fabricating novel fibre Bragg gratings and integrated optical components. The inscription of waveguides in various transparent glasses using a femtosecond laser was first demonstrated in 1996, however the technique has only matured in recent years. We have inscribed uniform and chirped FBGs in silica and ZBLAN fibres using the core-scanned method, by controlling the movement of the fibre through the focus of a femtosecond laser beam. Mechanically robust FBGs could be fabricated into active ZBLAN fibre, without the need of any phasemasks and without the need to remove the jacket of the fibre. Later, these mechanically robust FBGs were used to develop a widely tunable all-fibre mid-IR laser system. Experimental results in this thesis demonstrated a tunability of 37 nm when applying mechanical tension or compression to the robust FBG. The results in this thesis present the first ever tunable all-fibre mid-IR laser by strain tuning a mechanically robust FBG inscribed through the polymer coating of a doped double-clad fluoride fibre. The efficiency of the all-fibre Fabry-Perot laser was further improved by inscribing a CFBG into the other end of the gain fibre thereby increasing the

cavity Q-factor. Fabricating integrated components such as directional couplers in mid-IR compatible glasses is a promising route for the construction of all-fibre ring laser systems. Our results have shown that ZBLAN glass is not well suited as material for these applications due to unavoidable and excessive losses at pump and signal wavelengths. In contrast, directional couplers fabricated in GLS glass show promising results that might pave the way for the construction of all-fibre ring laser cavities in the mid-IR region.

6.1 Future works

The obvious first step for future work is to improve the design of GLS couplers to achieve better coupling efficiency at 1150 nm and 2900 nm wavelengths and also use this coupler to build an efficient all-fibre mid-IR ring laser cavity. Moreover, these fabricated couplers could become a part of an integrated nonlinear fibre loop mirror to generate ultra-short pulses out of the oscillator [71]. In addition, chirped fibre Bragg gratings have a great potential to provide efficient dispersion management in laser cavities. Hence, the direct inscription of CFBGs into active ZBLAN fibres can aid the development of ultrafast laser sources with pulse durations down to the few-cycle regime.

To conclude, the development of mid-IR fibre laser is an important field of research that promises many applications spanning from fundamental molecular spectroscopy to next generation tools for laser surgery. It appears that the fabrication of femtosecond laser inscribed FBGs and integrated components could provide a platform from which the true benefit of environmentally stable and alignment free future mid-IR fibre laser systems can emerge. In this respect, the works detailed in this thesis represents an important contribution towards achieving mid-IR all-fibre laser cavities not only around 3 μm but also at longer wavelengths.

References

[1] J. Hao, P. Yan, and M. Gong. *Effect of mode competition on photodarkening distribution of Yb-doped fiber laser*. Optics Communications **287**, 167 (2013).

[2] D. D. Hudson. *Invited paper: Short pulse generation in mid-IR fiber lasers*. Optical Fiber Technology **20**(6), 631 (2014).

[3] T. Hu. *Ultrafast Mid-infrared Fibre Lasers*. PhD Thesis, University of Sydney (2015).

[4] S. Antipov, D. D. Hudson, A. Fuerbach, and S. D. Jackson. *High-power mid-infrared femtosecond fiber laser in the water vapor transmission window*. Optica **3**(12), 1373 (2016).

[5] C. B. Schaffer, A. Brodeur, and E. Mazur. *Laser-induced breakdown and damage in bulk transparent materials induced by tightly focused femtosecond laser pulses*. Measurement Science and Technology **12**(11), 1784 (2001).

[6] S. Gross. *Direct-write mid-IR waveguide lasers*. PhD Thesis, Macquarie University (2012).

[7] T. Gretzinger. *Towards Mid-IR 3D Integrated Optics for Astronomical Devices*. MRes Thesis, Macquarie university (2014).

[8] *https://www.hbm.com/en/6483/optical-fiber-sensors-vs-conventional-electrical-strain-gauges/* .

[9] R. J. Williams, N. Jovanovic, G. D. Marshall, G. N. Smith, M. J. Steel, and M. J. Withford. *Optimizing the net reflectivity of point-by-point fiber Bragg gratings : the role of scattering loss*. Optics Express **20**(12), 13451 (2012).

[10] Newport. *Fiber Optics : How Fused Fiber Optic Couplers Work*. Photonics Technical Note **25**, 1 (2014).

[11] S. Gross, N. Jovanovic, A. Sharp, M. Ireland, J. Lawrence, and M. J. Withford. *Low loss mid-infrared ZBLAN waveguides for future astronomical applications*. Optics Express **23**(6), 7946 (2015).

[12] A. Schliesser, N. Picqué, and T. W. Hänsch. *Mid-infrared frequency combs*. Nature Photonics **6**(7), 440 (2012).

[13] C. R. Petersen, U. Møller, I. Kubat, B. Zhou, S. Dupont, J. Ramsay, T. Benson, S. Sujecki, N. Abdel-Moneim, Z. Tang, D. Furniss, A. Seddon, and O. Bang. *Mid-IR supercontinuum covering the 1.4 μm to 13.3 μm molecular fingerprint region using ultra-high NA chalcogenide step-index fibre*. Nature Photonics **8**, 1 (2014).

[14] S. Antipov. *Towards ultrafast and ultra-broadband all-fibre laser systems for the mid-infrared*. PhD Thesis, Macquarie University (2017).

[15] A. Vogel, J. Noack, G. Hüttman, and G. Paltauf. *Mechanisms of femtosecond laser nanosurgery of cells and tissues*. Applied Physics B: Lasers and Optics **81**(8), 1015 (2005).

[16] B. E. A. Saleh and M. C. Teich. *Fundamentals of Photonics* (2007).

[17] X. Zhu and N. Peyghambarian. *High-power ZBLAN glass fiber lasers: Review and prospect*. Advances in OptoElectronics **2010** (2010).

[18] T. Hu, S. D. Jackson, and D. D. Hudson. *A Mid-Infrared Mode-locked Fiber Laser for Frequency Combs*. NLO 2015, OSA **1**, 8 (2015).

[19] V. Fortin, M. Bernier, S. T. Bah, and R. Vallée. *30 W fluoride glass all-fiber laser at 2.94 μm*. Optics Letters **40**(12), 2882 (2015).

[20] S. D. Jackson. *Towards high-power mid-infrared emission from a fibre laser*. Nature Photonics **6**(7), 423 (2012).

[21] R. Allen and L. Esterowitz. *CW diode pumped 2.3 μm fiber laser*. Applied Physics Letters **55**(8), 721 (1989).

[22] M. C. Brierley and P. France. *Continuous wave lasing at 2.7 μm in an erbium-doped fluorozirconate fiber*. Electronics Letters **24**(8), 935 (1988).

[23] O. Henderson-sapir, J. Munch, and D. J. Ottaway. *A Higher Power 3 . 5 μm Fibre Laser*. Advanced Solid State Lasers (ASSL) **OSA**, 5 (2014).

[24] L. Wetenkamp. *Efficient CW operation of a 2.9 μm Ho-doped fluorozirconate fibre laser pumped at 640 nm*. Electronics Letters **26**(8), 883 (1990).

[25] C. Carbonnier, H. Tobben, and U. B. Unrau. *Room temperature CW fibre laser at 3.22 μm*. Electronics Letters **34**(9), 893 (1998).

[26] J. Schneider, C. Carbonnier, and U. B. *Characterization of a Ho-doped fluoride ber laser with a 3.9 μm emission wavelength*. Applied Optics **36**(33), 8595 (1997).

[27] M. R. Majewski and S. D. Jackson. *Highly efficient mid-infrared dysprosium fiber laser*. Optics Letters **41**(10), 2173 (2016).

[28] D. Faucher, M. Bernier,G. Androz, N. Caron, R. Vallee. *20 W passively cooled single-mode all-fiber laser at 2.8 μm*. Optics Letters **36**(8), 1104 (2011).

[29] D. Hudson, E. Magi, L. Gomes, and S. Jackson. *1W diode-pumped tunable Ho:Pr-doped fluoride glass fibre laser*. Optics Letters **47**(8), 985 (2011).

[30] S. D. Jackson. *High-power and highly efficient diode-cladding-pumped holmium-doped fluoride fiber laser operating at 2940 nm*. Optics Letters **34**, 2327 (2009).

[31] O. G. Okhotnikov. *Fiber Lasers*. Wiley-VCH (10) (2012).

[32] T. Hu, S. D. Jackson, and D. D. Hudson. *Ultrafast pulses from a mid-infrared fiber laser*. Optics Letters **40**(18), 4226 (2015).

[33] V. Fortin, F Maes, M. Bernier, S. T. Bah, M D'auteuil and R. Vallee. *Watt-level erbium-doped all-fiber laser at 3.44 μ m*. Optics Letters **41**(3), 559 (2016).

[34] S. Tokita, M. Murakami, S. Shimizu, M. Hashida, and S. Sakabe. *12 W Q-switched Er:ZBLAN fiber laser at 2.8 μ m*. Optics Letters **36**(15), 2812 (2011).

[35] B. C. Stuart, M. D. Feit, S. Herman, A. M. Rubenchik, B. W. Shore, and M. D. Perry. *Nanosecond-to-femtosecond laser-induced breakdown in dielectrics*. Physical Review B **53**(4), 1749 (1996).

[36] J. W. Chan, T. R. Huser, S. H. Risbud, and D. M. Krol. *Modification of the fused silica glass network associated with waveguide fabrication using femtosecond laser pulses*. Applied Physics A **76**(3), 367 (2003).

[37] S. Gross, M. Dubov, and M. J. Withford. *On the use of the Type I and II scheme for classifying ultrafast laser direct-write photonics*. Optics Express **23**(6), 7767 (2015).

[38] D. J. Little, M. Ams, S. Gross, P. Dekker, C. T. Miese, A. Fuerbach, and M. J. Withford. *Structural changes in BK7 glass upon exposure to femtosecond laser pulses*. Journal of Raman Spectroscopy **42**(4), 715 (2011).

[39] B. Poumellec, L. Sudrie, M. Franco, B. Prade, and A. Mysyrowicz. *Femtosecond laser irradiation stress induced in pure silica*. Optics Express **11**(9), 1070 (2003).

[40] L. Sudrie, M. Franco, B. Prade, and A. Mysyrowicz. *Writing of permanent birefringent microlayers in bulk fused silica with femtosecond laser pulses*. Optics Communications **171**(4), 279 (1999).

[41] E. N. Glezer and E. Mazur. *Ultrafast-laser driven micro-explosions in transparent materials*. Applied Physics Letters **71**(7), 882 (1997).

[42] C. B. Schaffer, A. O. Jamison, and E. Mazur. *Morphology of femtosecond laser-induced structural changes in bulk transparent materials*. Applied Physics Letters **84**(9), 1441 (2004).

[43] T. Gorelik, M. Will, S. Nolte, A. Tuennermann, and U. Glatzel. *Transmission electron microscopy studies of femtosecond laser induced modifications in quartz*. Applied Physics A: Materials Science and Processing **76**(3), 309 (2003).

[44] R. J. Williams, R. G. Krämer, S. Nolte, and M. J. Withford. *Femtosecond direct-writing of low-loss fiber Bragg gratings using a continuous core-scanning technique*. Optics Letters **38**(11), 1918 (2013).

[45] Darren D. Hudson, Robert J. Williams, Michael J. Withford and S. D. Jackson. *Single frequency fiber laser operating at 2.9 μm*. Optics Letters **38**(6), 2388 (2013).

[46] A. Arriola, S. Gross, T. Gretzinger, M. Ams, H. Ebendorff-Heidepriem, J. Sanghera, M. Ireland, P. Tuthill, and M. Withford. *Ultrafast laser inscribed waveguides for mid-infrared interferometry: Experimental study of suitable host materials*. The European Conference on Lasers and Electro-Optics **10** (2015).

[47] T. Gretzinger, S. Gross, M. Ams, A. Arriola, and M. J. Withford. *Ultrafast laser waveguide inscription in Gallium Lanthanum Sulfide*. Photonics and Fiber Technology 2016 (ACOFT, BGPP, NP) (2016).

[48] K. O. Hill, Y. Fujii, D. C. Johnson, and B. S. Kawasaki. *Photosensitivity in optical fiber waveguides: Application to reflection filter fabrication*. Applied Physics Letters **32**(10), 647 (1978).

[49] K. O. Hill and G. Meltz. *Fiber Bragg grating technology fundamentals and overview*. Journal of Lightwave Technology **15**(8), 1263 (1997).

[50] K. M. Davis, K. Miura, N. Sugimoto, and K. Hirao. *Writing waveguides in glass with a femtosecond laser*. Optics Letters **21**(21), 1729 (1996).

[51] S. J. Mihailov, C. W. Smelser, P. Lu, R. B. Walker, D. Grobnic, H. Ding, G. Henderson, and J. Unruh. *Fiber bragg gratings made with a phase mask and 800-nm femtosecond radiation.* Optics Letters **28**(12), 995 (2003).

[52] M. Bernier, D. Faucher, N. Caron, and R. Vallée. *Highly stable and efficient erbium-doped 2.8 μm all fiber laser*. Optics Express **17**(19), 16941 (2009).

[53] J. Y. Lee and S. N. Hwang. *Direct writing of fibre Bragg gratings by femtosecond laser*. Electronics Letters **40**(19) (2004).

[54] A. Martinez, I. Y. Khrushchev, and I. Bennion. *Direct inscription of Bragg gratings in coated fibers by an infrared femtosecond laser*. Optics Letters **31**(11), 1603 (2006).

[55] R. J. Williams, R. G. Krämer, S. Nolte, and M. J. Withford. *Femtosecond direct-writing of low-loss fiber Bragg gratings using a continuous core-scanning technique.* Optics Letters **38**(11), 1918 (2013).

[56] S. Antipov, M. Ams, R. J. Williams, E. Magi, M. J. Withford, and A. Fuerbach. *Direct infrared femtosecond laser inscription of chirped fiber Bragg gratings*. Optics Express **24**(1), 30 (2016).

[57] J. Colaizzi and M. J Matthewson. *Mechanical Durability of ZBLAN and Aluminum Fluoride-Based Optical Fiber*. Journal of Lightwave Technology **12**(8), 1317 (1994).

[58] G. A. Ball and W. W. Morey. *Compression-tuned single-frequency Bragg grating fiber laser*. Optics Letters **19**(23), 1979 (1994).

[59] M.R. Mokhtar, C.S. Goh, S.A. Butler, S.Y. Set, K. Kikuchi, D.J. Richardson and M. Ibsen. *Fibre Bragg grating compression-tuned over 110 nm*. Electronics Letters **39**(6), 509 (2003).

[60] E. Bélanger, B. Déry, M. Bernier, J.-p. Bérubé, and R. Vallée. *Long-term stable device for tuning fiber Bragg gratings*. Applied Optics **46**(16), 3189 (2007).

[61] A. Arriola, S. Mukherjee, D. Choudhury, L. Labadie, and R. R. Thomson. *Ultrafast laser inscription of mid-IR directional couplers for stellar interferometry*. Optics Letters **39**(8), 4820 (2014).

[62] D. G. Lancaster, S. Gross, H. Ebendorff-Heidepriem, K. Kuan, T. M. Monro, M. Ams, A. Fuerbach, and M. J. Withford. *Fifty percent internal slope efficiency femtosecond direct-written Tm:ZBLAN waveguide laser*. Optics Letters **36**, 1587 (2011).

[63] D. G. Lancaster, S. Gross, H. Ebendorff-Heidepriem, A. Fuerbach, M. J. Withford, and T. M. Monro. *2.1 μm waveguide laser fabricated by femtosecond laser direct-writing in Ho,Tm:ZBLAN glass*. Optics Letters **37**, 996 (2012).

[64] A. Saliminia, J.-P. Bérubé, and R. Vallée. *Refractive index-modified structures in glass written by 266nm fs laser pulses*. Optics Express **20**(25), 27410 (2012).

[65] S. Blair. *Technical note: Fiber connector losses* pp. 58–59.

[66] N. Carlie, N. C. Anheier, H. A. Qiao, B. Bernacki, M. C. Phillips, L. Petit, J. D. Musgraves, and K. Richardson. *Measurement of the refractive index dispersion of As_2Se_3 bulk glass and thin films prior to and after laser irradiation and annealing*

using prism coupling in the near- and mid-infrared spectral range. Review of Scientific Instruments **82**(5), 0 (2011).

[67] O. M. Efimov, L. B. Glebov, K. A. Richardson, E. Van Stryland, T. Cardinal, S. H. Park, M. Couzi, and J. L. Brunéel. *Waveguide writing in chalcogenide glasses by a train of femtosecond laser pulses*. Optical Materials **17**(3), 379 (2001).

[68] E. Romanova, A. Konyukhov, S. Muraviov, and A. Andrianov. *Thermal diffusion in chalcogenide glass irradiated by a train of femtosecond laser pulses*. 12th International Conference on Transparent Optical Networks,2010, ICTON 2010 pp. 26–29 (2010).

[69] T. Schweizer, D. Hewak, B. Samson, and D. Payne. *Spectroscopy of potential mid-infrared laser transitions in gallium lanthanum sulphide glass*. Journal of Luminescence **72-74**(96), 419 (1997).

[70] T. Gretzinger, S. Gross, M. Ams, A. Arriola, and M. J. Withford. *Ultrafast laser inscription in chalcogenide glass: thermal versus athermal fabrication*. Optical Materials Express **5**(12), 2862 (2015).

[71] N. J. Doran and D. Wood. *Nonlinear-optical loop mirror*. Optics Letters **13**(1), 56 (1988).

[72] K.O. Hill and G. Meltz. *Fiber Bragg grating technology fundamentals and overview*. J. Lightwave Technol. **15**, 1263–1276 (1997).

[73] S. Gross, M.Ams, G. Palmer, C.T. Miese, R.J. Williams, G.D. Marshall and A. Fuerbach. *Ultrafast Laser Inscription in Soft Glasses: A Comparative Study of Athermal and Thermal Processing Regimes for Guided Wave Optics*. Int. J. Applied Glass Science **3**, 332–348 (2012).